

Senescence of endothelial cells increases susceptibility to Kaposi's sarcoma-associated herpesvirus infection via CD109-mediated viral entry

Myung-Ju Lee¹, Jun-Hee Yeon¹, Jisu Lee¹, Yun Hee Kang^{1,2}, Beom Seok Park³, Joohee Park¹, Sung-Ho Yun⁴, Dagmar Wirth⁵, Seung-Min Yoo¹, Changhoon Park¹, Shou-Jinag Gao⁶, and Myung-Shin Lee^{1,2*}

¹ Department of Microbiology and Immunology, Eulji University School of Medicine, Daejeon, Republic of Korea

² Eulji Biomedical Science Research Institute, Eulji University School of Medicine, Daejeon, Republic of Korea

³ Department of Biomedical Laboratory Science, College of Health Science, Eulji University, Seongnam, Republic of Korea

⁴ Research Center for Bioconvergence Analysis, Korea Basic Science Institute (KBSI), Cheongju 28119, Korea.

⁵ Model Systems for Infection and Immunity, Helmholtz Centre for Infection Research, Braunschweig, Germany

⁶ Tumor Virology Program, UPMC Hillman Cancer Center, and Department of Microbiology and Molecular Genetics, University of Pittsburgh, Pittsburgh, PA, 15232, USA.

22 Authorship note: MJL and JHY contributed equally to this work as co–first authors.

23

24 * Corresponding author

25 Myung-Shin Lee

26 Address: Department of Microbiology and Immunology, Eulji University School of

27 Medicine, 77 Gyeryong-ro 771 beon-gil, Jung-gu, Daejeon, 34824, Republic of Korea

28 Telephone: +82 42 259 1662

29 E-mail: mslee@eulji.ac.kr

30

31 **Conflict of interest**

32 The authors have declared that no conflict of interest exists.

ABSTRACT

The aging process is characterized by cellular functional decline and increased susceptibility to infections. Understanding the association between virus infection and aging is crucial for developing effective strategies against viral infections in older individuals. However, the relationship between Kaposi's sarcoma-associated herpesvirus (KSHV) infection, a cause of increased Kaposi's sarcoma prevalence among the elderly without HIV infection, and cellular senescence remains enigmatic. This study uncovered a fascinating link between cellular senescence and enhanced KSHV infectivity in human endothelial cells. Through a comprehensive proteomic analysis, we identified caveolin-1 and CD109 as host factors significantly upregulated in senescent cells that promote KSHV infection. Remarkably, CRISPR-Cas9-mediated knockout of these factors reduced KSHV binding and entry, leading to decreased viral infectivity. Furthermore, surface plasmon resonance analysis and confocal microscopy revealed a direct interaction between KSHV virions and CD109 on the cell surface during entry, with recombinant CD109 protein exhibiting inhibitory activity of KSHV infection by blocking virion binding. These findings uncovered a previously unrecognized role of cellular senescence in enhancing KSHV infection through upregulation of specific host factors and provided insights into the complex interplay between aging and viral pathogenesis.

Introduction

Kaposi's sarcoma-associated herpesvirus (KSHV), also known as human herpesvirus 8 (HHV-8), is a member of the herpesvirus family. KSHV infection is associated with the development of Kaposi's sarcoma (KS), a vascular cancer that is particularly prevalent in immunocompromised individuals, including those with acquired immunodeficiency syndrome (AIDS) (1). KS is characterized by the formation of red or purple skin lesions, which can progress to involve the internal organs and cause serious complications. Classic KS is more common in older individuals, particularly those over the age of 50 years (2). The incidence of KS increases with age, and the disease is more aggressive and difficult to treat in older patients (3). This age-dependent pattern suggests a complex interplay between viral pathogenesis and the aging process, the mechanisms of which remain elusive.

Human immunodeficiency virus (HIV) infection is one of the most important risk factors for KS (4). HIV infection has been associated with an increased risk of age-related diseases, including cardiovascular disease, neurocognitive impairment, and certain cancers (5, 6). Cellular senescence, a hallmark of aging, has been proposed as a potential factor in the pathogenesis of various age-related diseases (7, 8). Some studies have suggested that HIV infection may influence various processes associated with cellular senescence (5, 9). HIV-induced oxidative stress and the direct effects of viral proteins, such as Tat, may contribute to premature cellular senescence (10). While the relationships among aging, HIV infection, and KS are complex and multifaceted, these findings highlight the potential impact of cellular senescence on KS. However, the specific

74 role of senescence in KSHV infection and KS development is yet to be established. Given
75 the age-dependent pattern of KS incidence and severity, understanding the relationship
76 between cellular senescence and KSHV susceptibility could provide valuable insights into
77 KS pathogenesis.

78 To address this knowledge gap, we investigated the susceptibility of senescent human
79 endothelial cells to KSHV infection using primary human endothelial cells (HUVECs) and
80 a conditionally immortalized human endothelial cell line containing doxycycline-controlled
81 SV40 large T antigen and hTERT-expressing cassettes (HuARLT cells) (11). We found
82 that senescent cells are more susceptible to KSHV infection than non-senescent cells.
83 Mass spectrometry analysis revealed differential expression of proteins between
84 senescent and non-senescent cells, of which four membrane proteins were examined for
85 their roles in the increased susceptibility of senescent cells to KSHV. Throughout
86 systematic examination involving the use of knockout clones and cells overexpressing
87 candidate proteins, we discovered that CD109 had an essential role in KSHV attachment
88 and infection in human endothelial cells, particularly in senescent cells.

Results

Cellular senescence enhances KSHV infectivity in human endothelial cells. To investigate the infectivity of KSHV in senescent human endothelial cells, we employed three established senescence models: replicative senescence in HUVECs through extended passaging (> 35 passages), doxorubicin-induced senescence in HUVECs (12, 13), and doxycycline withdrawal-induced senescence in HuARLT cells (11) (Figure 1A). The senescent status of HUVECs and HuARLT cells was analyzed by SA- β -gal, Western-blotting, and cell proliferation. Cultures induced for senescence by all three methods had increased SA- β -gal-positive cells (Figure 1A and Supplemental Figure 1A), and increased expression levels of p16 or p21 proteins (Supplemental Figure 1B). After 35 passages, senescent HUVECs had a lower rate of cell division compared with the early-passage cells (Supplemental Figure 1C). Similarly, senescent cells derived from both doxycycline-withdrawn HuARLT cells and doxorubicin-treated HUVECs exhibited diminished cell proliferation compared with their non-senescent control cells (Supplemental Figure 1D). In cell cycle analysis, all senescent cells demonstrated decreased S phase cells (Supplemental Figure 1E). Together, these results confirm that all three approaches effectively triggered cellular senescence in human endothelial cells.

To assess the ability of senescent cells to support KSHV infection, the three types of senescent cells were infected with recombinant KSHV BAC16. Since senescent cells stop dividing, equal numbers of senescent and non-senescent cells were seeded one day prior to infection to minimize differences in cell number. The next day, equal amounts of virus were used to infect cells, aiming to produce 10-30% of GFP positive cells in non-

senescent cells. Because recombinant KSHV BAC16 contains a GFP cassette, we monitored KSHV infection based on the expression of GFP protein at day 1 postinfection (14). All three types of senescent endothelial cells showed significantly higher levels of KSHV infection than their non-senescent control cells (Figure 1B and Supplemental Figure 2). These results were confirmed by staining for the expression of KSHV latent protein LANA in the infected cells (Supplemental Figure 3). In agreement with these results, higher copy numbers of viral genomes and higher expression levels of viral latent gene *ORF71* were detected in KSHV-infected senescent than non-senescent cells (Figure 1, C and D). We investigated whether senescent cells experienced a different outcome after infection with KSHV by examining their viability and the expression of viral lytic cycle genes at day 4 postinfection. Intriguingly, after KSHV infection, the number of dead cells was significantly increased in senescent HUVECs and HuARLT cells compared to non-senescent cells (Supplemental Figure 4, A and B). In senescent cells, mRNA and protein expressions of lytic genes of KSHV were significantly increased (Supplemental Figure 4, C and D). Furthermore, we found that virus production was also increased in senescent cells (Supplemental Figure 4E). These findings indicate that senescent cells are more susceptible to KSHV infection and support a higher level of viral lytic replication. Because of the challenges in maintaining a large quantity of HUVECs in replicative senescence state, we primarily performed our subsequent experiments with doxorubicin-treated HUVECs and doxycycline-withdrawn HuARLT cells.

Increased KSHV entry and binding in senescent endothelial cells. To determine whether senescence might affect KSHV entry and trafficking, we examined KSHV particles by staining the viral capsid protein ORF65 at 4 hours postinfection (hpi) (Figure 2, A and B, and Supplemental Figure 5). A previous study has shown that KSHV particles dock at perinuclear regions following successful entry into and trafficking in cells (15). We found significantly more KSHV particles in perinuclear regions in senescent HUVECs and HuARLT cells than non-senescent control cells. Additionally, we detected higher copy numbers of KSHV genomic DNA in senescent than non-senescent cells (Figure 2C). These results indicate that senescence might facilitate KSHV entry and trafficking.

To investigate whether the enhanced KSHV entry and trafficking in senescent cells was due to increased binding of virions on the cell surface, we infected the cells with KSHV virions for 1 hour at 4°C. We then examined the virions by staining for KSHV envelope glycoprotein K8.1 without a permeabilization process (Figure 3, A and B, and Supplemental Figure 6). We found that KSHV binding to the cell surface was significantly increased in senescent cells compared to non-senescent cells. Thus, the increased KSHV infectivity in senescent cells might be in part due to the enhanced binding of virions to the cell surface. To confirm these results, we isolated KSHV-infected cells at 1 hpi through a scraping and washing procedure. DNA was then extracted and quantified for viral genome copy numbers (Figure 3C). We detected higher viral genomic copy numbers in senescent than non-senescent cells. Thus, senescence might promote KSHV infection by enhancing binding of virions to the cells.

KSHV enters host cells through a multistep process that involves interactions between viral envelope glycoproteins and host cell surface receptors. Several endothelial cell surface proteins have been identified as potential entry receptors for KSHV, including integrins, heparan sulfate proteoglycan (HSPG), and ephrin type-A (EphA) receptors (16). To investigate whether the expression of known receptors for KSHV entry was changed in senescent cells, we analyzed their expression levels by flow cytometry (Supplemental Figure 7). In HUVECs, the expression levels of numerous known KSHV entry receptors, such as EphA2 and integrin $\alpha V\beta 5$, were increased in senescent cells compared to non-senescent cells. However, no known KSHV entry receptors were increased in senescent HuARLT cells. In contrast, numerous KSHV entry receptors, such as HSPG, xCT, and CD98, had reduced surface expression in senescent HuARLT cells compared to non-senescent cells. Given these observations, there may be additional host factors responsible for the elevated susceptibility to KSHV infection in senescent endothelial cells.

Identification of membrane proteins associated with increased KSHV infectivity in senescent cells. To identify host factors that might enhance KSHV infectivity in senescent human endothelial cells, we compared the differential protein expression between non-senescent and senescent HuARLT cells by SDS-PAGE (Supplemental Figure 8). Because of the enhanced binding of KSHV in senescent cells (Figure 3, A-C), we analyzed both the soluble (cell lysate) and insoluble (cell pellet) fractions after protein lysis to ensure the inclusion of all membrane proteins. After Coomassie blue staining of the SDS-PAGE gel, we observed variations in protein expression between uninfected

senescent and non-senescent cells. LC-MS/MS revealed differentially expressed proteins between senescent and non-senescent cells (Figure 4A and Table 1). A total of 6,575 proteins were identified in LC-MS/MS analysis. Of these, 303 proteins were increased more than 2-fold in the lysate of senescent cells compared to control cells. In addition, 45 proteins were increased more than 2-fold in the pellet from senescent cells compared to control cells. Following a thorough analysis of the LC-MS/MS data, seven membrane proteins were chosen as potential host factors that could enhance KSHV infection in senescent endothelial cells (Table 1). To confirm the differential expression of the candidate proteins in control and senescent cells, they were analyzed by Western-blotting (Figure 4B). Higher expression levels of all candidate proteins, except VASP, were observed in senescent HuARLT cells compared with control cells. Cell surface expression was analyzed in HuARLT cells and HUVECs using flow cytometry (Figure 4C and Supplemental Figure 9). The proteins that were increased in both senescent HuARLT cells and doxorubicin-treated HUVECs compared to their control cells included caveolin-1, integrin α 2, F11R, and CD109. The expression rate of F11R was >100% in both non-senescent and senescent cells compared to the isotype controls in flow cytometry, but senescent cells had higher expression levels (Supplemental Figure 9).

Establishment and characterization of knockout clones for the candidate proteins in HuARLT cells. To investigate whether the candidate proteins are associated with enhanced infection of senescent cells by KSHV, we performed knockout of these proteins in HuARLT cells using the CRISPR-Cas9 technology. Two single-guided RNAs (sgRNAs)

for each target protein were used and the most effective one was then selected (Figure 5A). Each clone was then isolated by limiting dilution, and the knockout clone was chosen based on the target protein expression by Western-blotting (Figure 5B). To analyze the mutated sequences in these clones, we cloned the PCR products, which contained the sgRNA-targeted region, into a T-cloning vector. Subsequently, we isolated 10 separate colonies and analyzed their sequences by Sanger sequencing. For *CAV1*, we found that all colonies exhibited a single nucleotide deletion at the Cas9 targeting site (Figure 5C). In the case of *ITGA2*, eight colonies had a 5-nucleotide deletion and two colonies had a 72-bp insertion at the Cas9 targeting site (Figure 5C), indicating that two alleles had different mutations. For both *F11R* and *CD109*, all colonies demonstrated the addition of a single nucleotide at the Cas9 targeting site (Figure 5C). Although cell proliferation rates of *ITGA2* and *CD109* knockout cells did not change, those of *CAV1* and *F11R* knockout cells were significantly reduced compared to the wild-type cells (Supplemental Figure 10A). To examine whether senescence could still be induced in the knockout cells, we withdrew doxycycline from HuARLT cells and then performed the SA- β -gal assay and assessed p21 expression. We observed SA- β -gal staining and p21 expression following the induction of senescence in all types of knockout cells, which was comparable to that seen in WT cells (Supplemental Figure 10, B and C).

Identification of crucial host factors for KSHV infection using knockout cell clones. To evaluate the role of each candidate protein in KSHV infection, we infected the wild-type and knockout cells, with or without induction of senescence. We employed 1 GFP

infectious unit, which infected approximately 90% of non-senescent wild-type cells. Additional cells were infected with 2-fold serially diluted virus. Similar to the results shown in Figure 1, senescent wild-type cells demonstrated higher viral infectivity than the non-senescent cells (Figure 6, A and B). Knockout of *CAV1* and *CD109* inhibited KSHV infection in both non-senescent and senescent cells. These results were confirmed by flow cytometric analysis (Figure 6, C and D, and Supplemental Figure 11). In contrast, knockout cells for *ITGA2* and *F11R* did not affect viral infectivity (Figure 6, A-D). We observed a sigmoid pattern of infectivity with serially diluted viruses (Supplemental Figure 11). At 1 GFP infectious unit, non-senescent wild-type cells had approximately 90% infection rate, which was reduced to less than 50% following *CAV1* knockout. Senescent cells also exhibited a significant difference in infectivity between wild-type and *CAV1* knockout cells (95% vs. 76%). At lower GFP infectious units (0.5 and 0.25), both non-senescent and senescent cells exhibited a significant difference in KSHV infectivity between wild-type and knockout cells (Figure 6, C and D). *CD109* knockout cells presented a notable difference in infectivity compared to wild-type cells with or without induction of senescence (Figure 6, C and D). In contrast, knockout of *ITGA2* and *F11R* did not affect infectivity in both senescent and non-senescent cells at all the GFP infectious units tested (Figure 6, C and D, and Supplemental Figure 11). Taken together, these results indicate that caveolin-1 and CD109 are potential factors regulating KSHV infectivity. Importantly, we detected higher expression levels of both caveolin-1 and CD109 in replicative senescent HUVECs than non-senescent cells (Supplemental Figure 12). Results of several previous studies demonstrated that caveolin-1 expression significantly increased with age in vivo and in vitro, which are consistent with our

observations (17-19). While the relationship between aging and caveolin-1 expression is well established, emerging evidence also supports an age-dependent regulation of CD109 expression in vivo. Transcriptomic analyses across multiple tissues in *Macaca fascicularis* revealed consistent age-associated increases in *CD109* RNA expression, which were particularly prominent in endothelial cells, with the exception of retinal tissue. Although human studies were more limited in scope, transcriptional profiling of skin fibroblasts and HUVECs demonstrated similar age-dependent elevation of *CD109* expression (Table 2). Mechanistic insights into this age-associated regulation have emerged from studies of cellular senescence. Notably, human mesenchymal stem cells lacking the anti-aging gene *WRN* exhibit increased *CD109* expression concurrent with cellular senescence. The causality of this relationship was further supported by the observation that treatment with quercetin, an anti-aging compound, reduced *CD109* expression by 23% in these senescent cells (20). To validate these findings in human tissues, we performed immunohistochemical analyses comparing endothelial CD109 expression between neonatal and elderly tissue specimens. Our results demonstrated significantly elevated CD109 expression in aged endothelial cells (Supplemental Figure 13), providing direct evidence for age-associated CD109 upregulation in vivo. These findings, supported by both molecular and histological evidence, established CD109 as an age-regulated protein with potential implications for age-associated KSHV susceptibility.

To further confirm the roles of caveolin-1 and CD109 in KSHV infectivity, we examined binding of KSHV virions to the cell surface by staining for KSHV K8.1 proteins in *CAV1* and *CD109* knockout cells (Figure 7, Supplemental Figure 14). We observed viral

particles on the cell surfaces of both non-senescent and senescent wild-type cells, with significantly more particles observed on senescent cells (Figure 7, A and B). However, knockout of either *CAV1* or *CD109* significantly decreased the number of viral particles on the cell surfaces. Similarly, knockout of either *CAV1* or *CD109* also reduced genomic DNA of KSHV virions on the cell surface compared to wild-type cells (Figure 7C).

Assessment of KSHV interaction with CD109 and caveolin-1. We further examined whether KSHV virions directly bind to CD109 and caveolin-1 during infection of senescent HuARLT cells (Figure 8, A-C). Confocal microscopy confirmed that KSHV virions revealed by KSHV K8.1 protein staining were distributed on the cell surface and colocalized with CD109 but not caveolin-1 on HuARLT cell surface within 1 hpi (Figure 8, A-B and Supplemental Figure 15). The calculated Manders' colocalization coefficients also support these findings (Figure 8C). These results indicate that K8.1 protein on KSHV virions directly binds to CD109 but not caveolin-1 on the cell surface. To confirm the role of CD109 in mediating binding of KSHV virions to the cell surface during infection, we established stable CD109 and caveolin-1 cell lines in 293T cells (Supplemental Figure 16, A and B). KSHV infectivity was increased in cells overexpressing CD109 but not caveolin-1 (Supplemental Figure 16, C and D). As expected, overexpression of CD109 but not caveolin-1 enhanced the cell surface binding of KSHV genomic DNA (Supplemental Figure 16E). To confirm the direct binding of KSHV virions to CD109 protein, a recombinant CD109 protein was immobilized on the sensor chip for surface plasmon resonance (SPR) analysis. KSHV virions bound to CD109-immobilized sensor chip in a

dose-dependent manner when introduced at three different concentrations in the running buffer (Figure 8D). Furthermore, when recombinant CD109 and KSHV virions were mixed and used for infection, we observed a decrease in KSHV infection rate proportional to the amount of recombinant CD109 added (Figure 8E). These findings indicate that recombinant CD109 inhibits KSHV infection by blocking bindings of KSHV virions to the cell surface. Hence, KSHV virions directly bind to CD109 during entry into cells, and the enhanced expression of CD109 in senescent cells promotes KSHV entry and infection.

CD109 specifically interacts with KSHV gH/gL glycoproteins. To identify the specific viral glycoproteins mediating the interaction with CD109, we generated KSHV glycoproteins tagged with either 3xHA (gB, gH, K8.1) or GFP (gL). Co-immunoprecipitation analyses revealed that the gH/gL heterodimer specifically interacts with CD109, while no binding was detected with either gB or K8.1 glycoproteins (Figure 9). This finding is consistent with the surface plasmon resonance results showing direct binding between CD109 and intact KSHV virions, and specifically identifies the gH/gL complex as the viral binding partner for CD109.

Discussion

In this study, we have found that senescent human endothelial cells are more susceptible to KSHV infection. This heightened susceptibility is associated with the increased expression of CD109 and caveolin-1 proteins in senescent cells compared to their non-senescent counterparts. In particular, CD109 directly mediates the binding of KSHV virions to the cell surface during infection. The virus enters host cells through a multistep process involving interactions between viral envelope glycoproteins and host cell surface receptors. Several host cell surface receptors have been identified as potential entry receptors for KSHV (16). Integrins are transmembrane receptors responsible for facilitating cell adhesion and signaling processes. They have been shown to interact with KSHV envelope glycoprotein gB (21, 22). HSPGs are glycosaminoglycan chains that are attached to cell surface proteoglycans and have been shown to interact with glycoproteins K8.1 and gH alone, and the gH/gL complex (23). EphA receptors are a family of transmembrane proteins involved in cell signaling and have been shown to interact with the gH/gL complex (24, 25). Our identification of the direct interaction between CD109 and the gH/gL glycoprotein complex provides insights into mechanisms of KSHV entry into cells. Our results show that the gH/gL heterodimer uses CD109 as a binding receptor in addition to the previously identified HSPGs and EphA, suggesting the complexity of KSHV cell entry mechanisms. This raises intriguing questions about how these distinct receptor-glycoprotein interactions might cooperate to facilitate KSHV infection. Further investigation of the potential interplay among CD109, HSPGs, EphA receptors, and the gH/gL complex will be crucial for a full understanding of the molecular mechanisms of KSHV entry into cells.

328 Our study demonstrated critical roles of CD109 and caveolin-1 in KSHV infection.
329 Caveolin-1 is a membrane protein and most of its protein structures are embedded within
330 the cell membrane (26), making it impossible for it to directly interact with KSHV virions
331 on the cell surface. Our findings indicated that overexpressing caveolin-1 did not lead to
332 increased KSHV infectivity, implying that KSHV virions are unlikely to directly bind to
333 caveolin-1 on the cell surface. However, KSHV infectivity significantly decreased in
334 caveolin-1 knockout cells, suggesting that caveolin-1 is an essential factor for KSHV
335 infection by regulating other step(s) of KSHV infection. Caveolin-1, while renowned for its
336 diverse cellular functions including signal transduction, lipid homeostasis, and tumor
337 suppression, plays an indispensable role in caveolin-mediated endocytosis. Previous
338 studies have established that KSHV can enter cells through multiple pathways, depending
339 on the cell type. In human dermal microvascular endothelial cells (HMVEC-d), studies
340 have demonstrated that KSHV primarily uses macropinocytosis as its major route of cell
341 entry (27), whereas lipid rafts play a critical role in KSHV infection in these cells (28).
342 Greene and Gao demonstrated that in HUVECs, KSHV cell entry is involved with clathrin-
343 mediated endocytosis (15). Additionally, in monocytic THP-1 cells, caveolin-mediated
344 endocytosis has also been implicated in KSHV cell entry (29). Our study adds to this
345 complex picture of KSHV internalization in endothelial cells. The interaction between
346 CD109 and caveolin-1, as reported by Bizet et al. (30), suggests a potential mechanism
347 by which the caveolar pathway might facilitate KSHV cell entry. Given the role of caveolin-
348 1 in KSHV infection in this study, it is possible that CD109 acts as a receptor, potentially
349 concentrating virions near caveolae or facilitating their internalization via the caveolar
350 pathway. This hypothesis is consistent with our observation of increased KSHV infectivity

351 in senescent cells, which have increased levels of both CD109 and caveolin-1. Our
352 findings suggest a potential link of CD109 to the caveolar endocytic pathway during KSHV
353 cell entry, but the exact role of CD109 in directing KSHV virions to specific internalization
354 routes needs to be clarified.

355 CD109 is a cell surface glycoprotein expressed in various cell types (31), including
356 endothelial cells (32). Its complex functions vary with cell type and cellular context. One
357 of its roles is to regulate the transforming growth factor-beta (TGF- β) signaling pathway
358 by binding to and blocking the TGF- β receptor, preventing downstream signaling (30, 33).
359 Previous studies have demonstrated that KSHV modulates TGF- β signaling through
360 multiple mechanisms: KSHV-encoded LANA inhibits TGF- β signaling by binding to the
361 promoter region of the TGF- β type II receptor (34), and KSHV miRNAs directly target
362 TGF- β pathway components (35-37). Given the pro- and anti-tumorigenic effects of TGF-
363 β in tumor progression (38, 39), further studies are needed to elucidate whether the
364 KSHV-CD109 interaction represents an additional mechanism by which KSHV regulates
365 TGF- β signaling during infection and KS development, particularly in the context of
366 cellular senescence and aging.

367 Aging is generally associated with an increase in the number of senescent cells in various
368 tissues (40). This can lead to a gradual decline in immune function, making older
369 individuals more susceptible to certain viral infections (41). However, the association
370 between senescence and viral infection may be more complex than expected. The
371 interplay between senescence and viral infection is influenced by several factors,
372 including the virus type, host cell characteristics, and the specific infection context. While

373 senescence can act as a host defense mechanism against viral infections, some viruses
374 have evolved mechanisms to trigger senescence in host cells as a strategy to enhance
375 viral infection (42, 43). Previous research has demonstrated that KSHV can alter cellular
376 senescence in KSHV-infected cells through certain viral proteins (44-47). Based on
377 previous studies (44, 47), senescence might serve an antiviral or anticancer function
378 during KSHV infection. Contrary to this notion, we have shown that KSHV exploits
379 senescent endothelial cells to enhance lytic replication and virus production, rather than
380 bypassing senescence (Supplemental Figure 4). This finding is particularly relevant in the
381 context of KS, where a small number of cells undergoing spontaneous lytic replication are
382 considered critical for KSHV pathogenesis (48). Thus, senescent cells may serve as a
383 source of lytic replication among KSHV-infected cells, thereby contributing to the
384 progression of KSHV-associated cancers. While the precise mechanism of enhanced
385 KSHV lytic replication remains to be defined, it could be speculated that this might be due
386 to the high level of oxidative stress in the senescent cells (49). In fact, previous studies
387 have shown that oxidative stress can promote KSHV lytic replication (50-52).

388 Beyond cellular senescence, our investigation of CD109 expression extends to HIV
389 infection, where multiple independent studies suggest an association between HIV status
390 and CD109 upregulation. Transcriptional analysis of HIV-1 latency models,
391 encompassing both established cell lines (CA5, EF7, CG3) and primary T cells isolated
392 from HIV-infected patients (JWEAU-A10 and JWEAU-C6), revealed significantly elevated
393 CD109 gene expression compared to their uninfected counterparts (53). This relationship
394 is further supported by quantitative glycoproteomic profiling demonstrating a striking 30.5-
395 fold increase in CD109 protein expression in HIV-1-infected ACH-2 cells compared to

their uninfected parental A3.01 cells (54). A recent large-scale plasma proteomics analysis of 1,293 proteins identified CD109 among the top 10 proteins that correlated with cell-associated HIV-1 DNA levels, highlighting its potential role in HIV pathogenesis (55). These convergent findings from diverse experimental approaches suggest a robust biological link between HIV infection and CD109 expression, potentially contributing to the increased KSHV susceptibility observed in HIV-positive individuals.

The present study was the first to illustrate the impact of senescence on KSHV infection in endothelial cells. Nevertheless, this intriguing observation raises several questions regarding KSHV-infected senescent endothelial cells. Senescent cells typically bolster their antiviral response by upregulating specific genes associated with innate immunity. Thus, the unexpected increase in KSHV infectivity in senescent endothelial cells warrants further investigation. It would be valuable to explore alterations in the immune response to KSHV in these senescent cells. In addition, senescence has been implicated in cancer development and metastasis/dissemination by altering the tumor microenvironment (56, 57). Hence, examining cellular differentiation and tumor development in senescent lymphatic endothelial cells or mesenchymal stem cells could present an intriguing avenue for investigating KSHV-induced tumorigenesis.

In conclusion, our study identified host factors that facilitate KSHV entry and trafficking in human endothelial cells, particularly in senescent cells. These findings provide insights into the mechanisms underlying KSHV pathogenesis related to aging and reveal an alternative infection pathway for KSHV entry into human endothelial cells. Understanding these mechanisms may contribute to the development of targeted therapeutic strategies

418 for KSHV-associated malignancies, particularly in the aging and immunocompromised
419 populations.

420

Methods

Sex as a biological variable. We analyzed CD109 expression in human tissue samples from both young (placenta and umbilical cord) and elderly individuals. Although samples were collected from both males and females, sex was not considered as a biological variable.

Cell culture and reagents. HuARLT cells, generated by Dagmar Wirth's lab (11), were cultured in endothelial cell growth medium-2 (Promocell) with supplements and 2 µg/mL doxycycline (Sigma-Aldrich). HUVECs purchased from Promocell were cultured in endothelial cell growth medium-2 with supplements. All HUVECs used in this experiment underwent fewer than 10 passages, except for those subjected to the induction of replicative senescence. Lenti-X™ 293T cells were purchased from TaKaRa (TaKaRa) and cultured in high glucose Dulbecco's Modified Eagle's Medium supplied with 10% FBS (GeneDEPOT) and 1% antibiotics (Gibco). All cells were cultured in a humidified atmosphere containing 5% CO₂ at 37°C. The senescence of HuARLT cells was induced by culturing without doxycycline for 5 days, whereas the senescence of HUVECs was induced by treating the cells with 50 nM doxorubicin for 5 days. In both cases, sub-culturing was performed every 2 days while senescence was induced. Conversely, replicative senescence was prompted by prolonged cultivation of early-passage HUVECs. HUVECs were sub-cultured every 2 days until reaching passage 35.

SA-β-gal staining assay. Senescent HuARLT cells and HUVECs were seeded in 6-well plates at 1×10^5 cells per well. The Senescence β-Galactosidase Staining Kit (Cell Signaling Technology) was used according to the manufacturer's instructions. The stained cells were visualized and images captured using a TS100 inverted-phase microscope (Nikon). To quantify cells positive for SA-β-gal using flow cytometry, we utilized the CellEvent™ Senescence Green Flow Cytometry Assay Kit (Thermo Fisher) to stain senescent HuARLT cells and HUVECs following the manufacturer's instructions. Stained cells were analyzed using a Guava Flow Cytometer (Luminex).

Analysis of cell proliferation. To evaluate cell proliferation in both non-senescent and aged endothelial cells, we employed the trypan blue exclusion assay to count HuARLT cells and HUVECs while inducing senescence. To determine the population doubling level in replicatively senescent HUVECs, cell counts were performed daily during sub-culturing. The population doubling level (PDL) was calculated using the following formula: $PDL = \text{initial PDL} + 3.322 \times (\log(\text{final cell count}) - \log(\text{initial cell count}))$.

Cell cycle analysis. Cells were detached from culture using Trypsin-EDTA (Gibco) and counted using Trypan-blue exclusion method. The cells were then adjusted to 5×10^5 cells in culture medium and washed with 1 ml of phosphate buffered saline (PBS). The cells were fixed with ice-cold 70% ethanol and incubated overnight at -20°C . Following fixation, the cells were permeabilized with 0.25% Triton-X 100 for 30 min at 4°C . The cells were then stained with $20 \mu\text{g/mL}$ of propidium iodide (Sigma-Aldrich) and $10 \mu\text{g/mL}$ of RNase

in PBS for 30 min at room temperature. The stained cell was analyzed using a Guava Flow Cytometer (Luminex).

KSHV isolation and infection. KSHV was isolated from iSLK BAC16 cells containing the recombinant KSHV BAC16 genome using a previously described method (58). KSHV infection of endothelial cells was achieved as described previously with some modifications (59). Briefly, senescent or non-senescent cells were seeded in a 6-well plate at 2×10^5 cells per well 1 day prior to infection. The cells were then washed with PBS and the medium replaced with Opti-MEM (Gibco) containing the same amount of KSHV per group and 5 $\mu\text{g/mL}$ polybrene (Santa Cruz Biotechnology). The plate was then centrifuged for 1 hour at $2,000 \times g$ and 25°C . Finally, the virus-containing media was replaced with fresh culture medium.

Analysis of KSHV-infected cells by fluorescence microscopy and flow cytometry. The KSHV-infected cells were evaluated for the expression of green fluorescent protein (GFP), which indicates infection. For imaging, cells expressing GFP were observed and photographed using an inverted fluorescence microscope (TS100, Nikon). Each test group was photographed three times and representative data were presented. For flow cytometry, infected cells were detached using trypsin-EDTA (Gibco), neutralized with endothelial cell growth medium-2 (Promocell), washed with 1 mL PBS, and resuspended in 500 μL PBS before analysis by a Guava Flow Cytometer (Luminex). Non-senescent endothelial cells were used to titer the concentration of infectious KSHV. Experimentally,

after establishing infectious titers that show about 10~30% of GFP-positive cells in non-senescent cells, the degree of KSHV infection was compared and analyzed in both non-senescent and senescent cells by infecting them with the same titer of the virus. In the case of KSHV infection comparative analysis in KO cells, with a titer showing about 90% infection in non-senescent wild-type cells set as 1 GFP infectious unit, 2-fold serially diluted virus was prepared and used to infect each prepared cell.

Quantification of viral genome or mRNA in KSHV-infected cells. One day prior to KSHV infection, control and senescent cells were seeded in 6-well plates at 2×10^5 cells per well. To quantify the internalized viral genomic DNA, 4 hours after infection, the cells were washed with PBS and then detached using trypsin-EDTA. The total DNA was extracted from the cells using the DNeasy kit (Qiagen) and normalized to a consistent concentration per volume using NanoDrop One (Thermo Fisher). For analysis of viral mRNA expression, RNA was extracted from infected cells 1 day postinfection using Ribospin™ (Geneall). The RNA concentration was standardized across samples by quantifying with NanoDrop. Subsequently, the standardized RNA was subjected to reverse transcription using TaKaRa 5X RT master mix (Takara). Real-time PCR was carried out with TaKaRa TBGreen fast qPCR mix (Takara). Amplification for human glyceraldehyde 3-phosphate dehydrogenase (GAPDH) was used as a housekeeping gene for normalization. The cycle conditions were 95°C for 30 s, followed by 40 cycles of 95°C for 5 s and 60°C for 10 s. The primers used in this experiment were KSHV *ORF26* gene, 5'-GGA GAT TGC CAC CGT TTA-3' (sense) and 5'-ACT GCA TAA TTT GGA TGT AGT C-3' (anti-sense); KSHV

ORF71 gene, 5'-GGA TGC CCT AAT GTC AAT GC-3' (sense) and 5'-GGC GAT AGT GTT GGG AGT GT-3' (anti-sense); and *GAPDH*, 5'-GGT ATG GTG GAA GGA CTC-3' (sense) and 5'-GTA GAG GCA GGG ATG ATG-3' (anti-sense), which were synthesized at Genotech. Specificity of the primers was confirmed by melting curve analysis.

Immunofluorescence and confocal image analysis. To analyze the binding of KSHV to the cellular surface, we employed a modified method based on Bottero et al (60). In the confocal microscopy assay, 1×10^5 cells were seeded on coverslips within a 24-well plate. The following day, each sample was infected with an equivalent volume of KSHV as described above. After the infection process, the infected cells were washed three times with PBS and immediately fixed with 4% paraformaldehyde for 30 minutes. With the exception of permeabilization steps, the sample preparation for confocal microscopy followed the IFA procedure (58, 61). Stained coverslips were mounted onto glass slides and analyzed using a ZEISS LSM 880 confocal microscope (ZEISS), with subsequent analysis by ZEISS Zen Blue Edition software. Particles were quantified using Nikon NIS software (Nikon). For quantifying KSHV particles internalized by cells postinfection, cells were incubated under 5% CO₂ at 37°C for 4 hours. Further staining was performed as described in the IFA method (58, 61). Stained cells were visualized by an E300 fluorescence microscope (Nikon). Images and particle counts were analyzed by Nikon NIS software (Nikon). Mouse anti-KSHV K8.1 antibody (1:100 dilution; SC-65446; 4A4; Santa Cruz Biotechnology), rabbit anti-caveolin-1 (1:100 dilution; A1555; Abclonal), rabbit anti-CD109 (1:100 dilution; 486955; E8L2W; Cell Signaling Technology), rat anti-LANA

(1:100 dilution; Ab4103; LN53; Abcam) and mouse anti-KSHV ORF 65 (1:100 dilution) (62) were used as primary antibodies. Alexa Fluor 568 phalloidin (Thermo Fisher) was used to stain F-actin. Alexa Fluor 568-conjugated anti-rat IgG (1:100 dilution; A11077; Thermo Fisher), Alexa Fluor 488-conjugated anti-mouse IgG antibody (1:100 dilution; A11001; Thermo Fisher), and Alexa Fluor 568-conjugated anti-mouse IgG antibody (1:100 dilution; A11004; Thermo Fisher) were used as secondary antibodies. Tris-buffered saline with 0.1% Tween 20 was used for the washing process after the antibody treatment. Nuclei were stained with 4',6-diamidino-2-phenylindole (DAPI). In the case of DAPI and phalloidin, they were used after secondary antibody treatment. To analyze colocalization, we performed quantitative colocalization analysis using Fiji software and applied the Colocalization Threshold plugin to calculate the Manders' colocalization coefficient (R). A maximum coefficient value of "1" indicates perfect overlap, whereas a minimum value of "0" represents complete exclusion.

Analysis of copy number of KSHV genome. The counting of KSHV genome copy number was conducted using a previously described method (63). One day prior to infection, 2×10^5 cells were seeded into each well of a 6-well plate. Following the procedure outlined above, the cells were infected. One day postinfection, the cells were washed twice with PBS and then cultured under the desired conditions. The supernatant containing KSHV particles was collected after the culture period for a set duration. This supernatant was treated with DNase RQ1 RNase-Free DNase (Promega) according to the manufacturer's instructions to remove free DNA, and the DNA within the virion was extracted using the

DNeasy kit (Qiagen). For quantification, a standard was established using pUC19 containing KSHV *ORF26*. The target sample and 10-fold serial diluted standards were quantified using the TaKaRa TBGreen Fast qPCR Mix (Takara), following the aforementioned procedure. The DNA quantity was determined using a series of standards with an R^2 value over 0.99.

Quantitative PCR analysis of KSHV binding and entry into host cells. The modified method previously described by Bottero et al (60) was used to determine the relative binding and entry of KSHV virions. HuARLT cells and HUVECs were seeded in a 6-well plate at 2×10^5 cells per well. To assess KSHV binding to host cells, they were thoroughly washed with PBS three times after infection and detached by scraping. The detached cells were collected by centrifugation at 800xg and washed twice with PBS to eliminate any unbound viral particles. To evaluate KSHV entry into host cells, cells were seeded in 6-well plates at a density of 2×10^5 cells per well. The next day, the cells were infected with KSHV and then incubated under 5% CO_2 at 37°C for 4 hours. Following incubation, cells were washed three times with PBS and treated with trypsin-EDTA to detach the cells and eliminate any remaining virus. The detached cells were then washed with PBS in two additional centrifugation steps. DNA extraction and quantification of the KSHV genome were performed as described above.

SDS-PAGE, in-gel digestion, and sample preparation for LC-MS/MS. To prepare protein samples for analysis, 30 µg of each sample were separated by 12% SDS-PAGE and

stained with Coomassie Brilliant Blue R-250. The entire gel was then divided into eight sections according to the molecular weights of the proteins. The sliced gels were digested with trypsin (Promega, Madison, WI) for 16 h at 37°C after reduction with 10 mM dithiothreitol and alkylation of cysteines with 55 mM iodoacetamide. The digested peptides were recovered by an extraction solution containing 50 mmol/L ammonium bicarbonate, 50% acetonitrile, and 5% trifluoroacetic acid. The extracted tryptic peptides were dissolved in 0.5% trifluoroacetic acid prior to further fractionation by LC-MS/MS.

LC-MS/MS analysis. Tryptic peptide samples were loaded onto a 2G-V/V trap column (Waters, USA) for the enrichment of peptides and removal of chemical contaminants. Concentrated tryptic peptides were eluted from the column and directed onto a 10 cm x 75 µm i.d. C18 reverse phase column (PROXEON, Denmark) at a flow rate of 300 nL/min. Peptides were eluted using a gradient of 0-65% acetonitrile for 80 min. All MS and MS/MS spectra were acquired in a data-dependent mode using an LTQ-Velos ESI Ion Trap mass spectrometer (Thermo Fisher). Every complete MS scan (m/z range 300 to 2,000) focused on the most abundant precursor ions in the MS spectra. For protein identification, MS/MS spectra were analyzed by MASCOT (Matrix Science, <http://www.matrixscience.com>). The human protein sequence database (UniProt_proteome_hu) was downloaded from UniProt and used for protein identification. Mass tolerance of the parent or fragment ion was 0.8 Da. Carbamidomethylation of cysteine and oxidation of methionine were considered to be variable modifications of tryptic peptides in the MS/MS analysis.

596

597 *Flow cytometry.* Non-senescent and senescent cells were detached by trypsin-EDTA.
598 The detached cells were reacted with primary antibody for 30 minutes at 4°C. The primary
599 antibodies used were rabbit anti-xCT (1:100 dilution; A13685; Abclonal), anti-Ephrin A2
600 (1:100 dilution; A23177; Abclonal), anti-HO-1 (1:100 dilution; A1346; Abclonal), anti-
601 Caveolin-1 (1:100 dilution; A1555; Abclonal), anti-integrin $\alpha 2$ (1:100 dilution; A7629;
602 Abclonal), anti-P4HB (1:100 dilution; A0692; Abclonal), anti-F11R (1:100 dilution; A1241;
603 Abclonal), and anti-VASP (1:100 dilution; A8862; Abclonal); anti-CD109 (1:100 dilution;
604 486955; E8L2W; Cell Signaling Technology), anti-integrin $\alpha 3\beta 1$ (1:100 dilution; bs-1057R;
605 Bioss), anti-integrin $\alpha V\beta 3$ (1:100 dilution; bs-1310R; Bioss), and anti-integrin $\alpha V\beta 5$ (1:100
606 dilution; bs-1356R; Bioss); and mouse anti-CD98 (1:100 dilution; sc-59145; 4F2; Santa
607 Cruz). Following the reaction, the cells were washed twice with PBS and a secondary
608 antibody was added. The secondary antibodies used in this experiment were mouse
609 F(ab)2 IgG (H+L) APC-conjugated antibody (10 μ l/10⁶ cells; F0101B, R&D systems) and
610 rabbit IgG APC-conjugated antibody (10 μ l/10⁶ cells; F0111, R&D systems). The cells
611 were analyzed using a Guava Flow Cytometer (Luminex).

612

613 *Establishment of knockout clones.* Knockout clones were obtained using the
614 CRISPR/Cas9 system following previously described methods with minor modifications
615 (61, 64). Briefly, TrueGuide synthetic sgRNA (Thermo Fisher) was used for gRNAs
616 against target genes: CRISPR639819_SGM (CCAGTATTTTCGTACAGTGA) for *CAV1*,
617 CRISPR956294_SGM (GGCTTTCCTGAGAACCGAAT) for *ITGA2*,

618 CRISPR830351_SGM (GGTCAAACCTTCCACTCCACA) for *F11R*, and
 619 CRISPR652545_SGM (CGGAGGAAATGTGACTATTG) for *CD109*. Each sgRNA and
 620 Truecut Cas9 protein v2 (Thermo Fisher) was transfected into HuARLT cells using
 621 Lipofectamine CRISPRMAX Cas9 transfection reagent (Thermo Fisher) following the
 622 manufacturer's instructions. After 2 days, the transfected cells were harvested, the cell
 623 concentration adjusted to 8 cells/mL, and the cells seeded into a 96-well plate at 100
 624 μ L/well to isolate a single clone. The sequencing analysis of DNA from the knockout
 625 clones followed the same method as described previously (61, 64). To analyze the
 626 sequences of each target gene, T-vector cloning was used with the following primers:
 627 CAV1 _S, 5'- TTC CCA AGT TCC AAG TGA TGC -3' (sense) and CAV1_AS, 5'- GGA
 628 ATA GAC ACG GCT GAT GC-3' (anti-sense) for *CAV1*; ITGA2_S, 5'- AAA GGC AGC
 629 AGG TCA AAT CA-3' (sense) and ITGA2_AS, 5'- AGA TGC GTG GAA AAT GTG CTA-
 630 3' (anti-sense) for *ITGA2*; F11R-S, 5'- AGT GCA CTC TTC TGA ACC TGA-3' (sense) and
 631 F11R_AS, 5'- CTC ATG GCC TTC CTA CCC C-3' (anti-sense) for *F11R*; and CD109_S,
 632 5'- TAA CAC AGG CCT TCC TCT AGT-3' (sense) and CD109_AS, 5'- ACC CTT CTG
 633 CAG TAA TAA CTG G-3' (anti-sense) for *CD109*. The reference sequences for *CAV1*,
 634 *ITGA2*, *F11R*, and *CD109* were based on specific regions of *Homo sapiens* chromosome
 635 5 (GRch38 primary assembly; 116,524,785 to 116,561,185; Entrez Gene ID 857),
 636 chromosome 5 (GRch38 primary assembly; 52,989,326 to 53,094,779; Entrez Gene ID
 637 3673), chromosome 1 (GRch38 primary assembly; 160,995,211 to 161,021,343; Entrez
 638 Gene ID 50848), and chromosome 6 (GRch38 primary assembly; 73,679,192 to
 639 73,828,317; Entrez Gene ID 135228), respectively.

640

641 *Cloning.* To clone KSHV glycoproteins gB-3xHA, gH-3xHA, K8.1-3xHA, and GFP-gL, we
642 first inserted a flexible linker (GGGGS) and 3xHA into the pcDNA3.1(+) vector using iPCR
643 (inverse PCR) to create the pcDNA3.1-3xHA construct. KSHV genomic DNA was
644 extracted from iSLK BAC16 cells and used as a template. The SLIC (sequence- and
645 ligation-independent cloning) method was employed to insert gB, gH, and K8.1 into
646 pcDNA3.1-3xHA, and gL was inserted into GFP-C1. First, pcDNA3.1-3xHA and each
647 glycoprotein were amplified to generate linear fragments with 40 bp homologous
648 sequences at both ends. Meanwhile, the GFP-C1 vector was linearized by digestion with
649 EcoRI and BamHI restriction enzymes. Subsequently, the linearized PCR products or
650 vector were mixed and incubated at room temperature for 2.5 minutes with T4 DNA
651 polymerase (Enzymomics). Following this, the DNA mixtures were kept on ice for 10
652 minutes and then transformed into competent *E. coli* cells. We also engineered FLAG-
653 CD109 purchased from Sino Biological into 3xFLAG-CD109 using iPCR. Prior to use, gB-
654 3xHA, gH-3xHA, K8.1-3xHA, 3xFLAG-CD109, and GFP-gL underwent DNA sequencing
655 analysis (Bionics) for verification.

656

657 *Co-immunoprecipitation assay.* To confirm the physical interaction between KSHV
658 glycoproteins and the CD109 receptor, co-Immunoprecipitation (co-IP) was performed.
659 Briefly, 50 μ L of anti-FLAG magnetic agarose beads (Pierce™, A36797) slurry was mixed
660 with 500 μ L of lysis buffer. The beads were collected using a magnetic stand, and the
661 supernatant was removed. This washing step was repeated three times. Next, 500 μ g of

662 cell lysate containing FLAG-tagged proteins was added to the beads and mixed, followed
663 by incubation at room temperature for 20 minutes with occasional vortexing. After
664 incubation, the beads were collected again and washed twice with 500 μ L of PBS buffer,
665 and finally washed with 500 μ L of purified water. To elute the immunoprecipitated
666 complexes, 100 μ L of 0.1M glycine buffer (pH 2.8) was added to the beads, which were
667 incubated at room temperature for 5 minutes with frequent vortexing. The supernatant
668 was collected, and 15 μ L of 1M Tris buffer (pH 8.5) was added to neutralize the pH. The
669 immunoprecipitated complexes were subsequently analyzed by Western blotting.

670

671 *Western blot analysis.* Western blot analysis was performed as described previously (63).
672 The primary antibodies were mouse-derived anti-p16 (1:1,000 dilution; sc-56330, JC8;
673 Santa Cruz), anti-p21 (1:1,000 dilution; sc-6246, F-5; Santa Cruz), anti-HHV-8 K8.1A/B
674 (1:1,000 dilution; sc-65446; 4A4; Santa Cruz), anti-KSHV ORF45 (1:1,000 dilution; MA5-
675 14769; 2D4A5; Thermo Fisher), anti-HA (1:1,000 dilution; 26183; Thermo Fisher), anti-
676 GFP (1:1,000 dilution; sc-9996; Santa Cruz). Anti-HO-1 (1:1,000 dilution; A19062;
677 Abclonal), anti-caveolin-1 (1:1,000 dilution; A19006; Abclonal), anti-integrin α 2 (1:1,000
678 dilution; A19068; Abclonal), anti-P4HB (1:1,000 dilution; A0692; Abclonal), anti-F11R
679 (1:1,000 dilution; A1241; Abclonal), anti-VASP (1:1,000 dilution; A0166; Abclonal), anti-
680 GAPDH (1:1,000 dilution; CSB-MA000071M0m; 14C2F11; Cusabio), anti-FLAG (1:1,000
681 dilution; F7425, Merck Millipore), and anti-CD109 (1:1,000 dilution; sc-271085; C-9; Santa
682 Cruz) antibodies were all of rabbit origin. The secondary reaction antibodies were goat
683 anti-mouse IgG heavy and light chain antibody HRP conjugated (1:5,000 dilution; A90-

116P; Bethyl Laboratories) and goat anti-rabbit IgG heavy and light chain antibody HRP-conjugated (1:5,000 dilution; A120-101P; Bethyl Laboratories). After all reactions, blots were captured by an Amersham ImageQuant 800.

Establishment of stable cell lines expressing caveolin-1 and CD109. To create cells that overexpress caveolin-1 and CD109, plasmids containing the specific target genes and control vectors were acquired from Sino Biological (Beijing, China). The plasmid vector was subsequently enriched within the *Escherichia coli* DH5 α system. Next, transfection of the plasmid vector into Lenti-X™ 293T cells was achieved using the Lipofectamine 3000™ (Thermo Fisher) in accordance with the manufacturer's instructions. Selection of the transfected cells was performed using 20 μ g/mL Hygromycin B (Thermo Fisher) over a span of 2 weeks. Prior to utilization, the success of the overexpression was validated by Western blotting.

Surface plasmon resonance (SPR) analysis. For SPR analysis, sensor chips comprising mixed self-assembled monolayers of 90% alkane-monothiol PEG3KOH and 10% alkane-monothiol PEG6K-COOH were mounted onto the instrument using immersion oil. The chip activation involved modifying the surface-free carboxyl groups by injecting a solution of 0.1 M 1-ethyl-3-(3-dimethylaminopropyl) carbodiimide hydrochloride and 0.05 M N-hydroxysuccinimide at a flow rate of 10 μ L/min to create a reactive succinimide ester surface. Recombinant human CD109 (R&D systems) (20 μ g/mL, prepared in 10 mM sodium acetate buffer, pH 5.0) was then coupled to the sensor via free amine coupling to

the immobilized succinimide, followed by quenching the remaining activated succinimide esters with 1 M ethanolamine, pH 8.5, to immobilize the ligand and block the chip. The association phase involved flowing a few μ M level analyte over the ligand-fixed channels at a flow rate of 30 μ L/min, and the dissociation phase was determined by flowing the running buffer at the same rate. To identify optimal regeneration conditions, 20 mM NaOH was injected as a regeneration solution after the association/dissociation steps at a flow rate of 30 μ L/min. KSHV was prepared in PBS (0.01 M phosphate buffer, 2.7 mM KCl, 0.137 M NaCl, pH 7.4) as the running buffer and serially diluted to achieve more than three concentrations. The association and dissociation times were set at 3 minutes each.

Virion neutralization assay. For the neutralization of KSHV by CD109 protein, the KSHV stock was mixed with recombinant human CD109 (4385-CD-050; R&D Systems) in PBS and incubated at 4°C for one hour with horizontal rotation to ensure thorough mixing. Following the incubation, HuARLT cells were infected with the virus-CD109 mixtures. At 24 hours of postinfection, the cells were detached using trypsin-EDTA and the infectivity was analyzed by measuring GFP expression using a Guava Flow Cytometer (Luminex).

Immunohistochemistry. Immunohistochemical staining was performed as previously described (62, 65) using rabbit polyclonal anti-CD109 antibody (1:100 dilution; 486955; Cell Signaling Technology) and alkaline phosphatase-conjugated goat anti-rabbit IgG (1:50 dilution; A3687; Sigma-Aldrich). Sections were developed with Vector Red AP substrate (Vector Laboratories) and counterstained with hematoxylin.

728

729 *Statistics.* All data shown in this paper were performed at least two times independently
730 and representative data are shown. In graphs, results are presented as the means \pm
731 standard deviations. To compare two different groups, two-tailed Student's t test was
732 used. For multiple comparisons to a single control group, Dunnett's test was performed
733 with Bonferroni correction to adjust for multiple testing. All data were considered
734 significantly different at a *P* value of <0.05 . Statistical significance of difference was
735 marked as asterisks: *, $P < 0.05$; **, $P < 0.01$ ***, $P < 0.001$.

736

737 *Study approval.* Human tissue samples were obtained with written informed consent from
738 all participants under protocols approved by the Institutional Review Board of Eulji
739 University Hospital (No. EMC 2021-06-007) in accordance with the Declaration of Helsinki.

740

741 *Data availability.* Values for all data points in graphs are reported in the Supporting Data
742 Values file. The mass spectrometry proteomics data have been deposited in the
743 ProteomeXchange Consortium (<http://proteomecentral.proteomexchange.org>) via the
744 PRIDE partner repository (<http://www.ebi.ac.uk/pride>) with the dataset identifier
745 PXD048212 (<http://www.ebi.ac.uk/pride/archive/projects/PXD048212>). Additional
746 detailed information is available from the corresponding author on request.

747 **Author Contributions**

748 MJL and MSL designed the study. MJL, JHY, JL, YHK, BSP, JP, SHY, and CP conducted
749 experiments. MJL, JHY, YHK, SMY, and MSL analyzed the data. MJL, YHK, and JHY
750 wrote the manuscript. MJL and JHY contributed to the experiments for the revision. DW,
751 SJG, and MSL reviewed and edited the manuscript. SJG and MSL supervised the study.
752 Co-first authors are listed in alphabetical order by last name.

753 **Acknowledgements**

754 This research was supported by the National Research Foundation of Korea (NRF),
755 project number NRF-2022R1I1A3065538 to MSL, a grant from the Korea Health
756 Technology R&D Project through the Korea Health Industry Development Institute
757 (KHIDI), funded by the Ministry of Health & Welfare, Republic of Korea (Grant No.
758 HV22C0181) to MSL. and the Basic Science Research Program of the NRF, funded by
759 the Ministry of Science, ICT & Future Planning (Grant No. RS-2024-00349208) to CP.
760 Graphical abstracted was created using BioRender.

761

References

1. Mesri EA, Cesarman E, and Boshoff C. Kaposi's sarcoma and its associated herpesvirus. *Nat Rev Cancer*. 2010;10(10):707-19.
2. Dal Maso L, Polesel J, Ascoli V, Zambon P, Budroni M, Ferretti S, et al. Classic Kaposi's sarcoma in Italy, 1985-1998. *Br J Cancer*. 2005;92(1):188-93.
3. Stiller CA, Trama A, Brewster DH, Verne J, Bouchardy C, Navarro C, et al. Descriptive epidemiology of Kaposi sarcoma in Europe. Report from the RARECARE project. *Cancer Epidemiol*. 2014;38(6):670-8.
4. Dittmer DP, and Damania B. Kaposi's sarcoma-associated Herpesvirus (KSHV)-associated Disease in the AIDS patient: An Update. *Cancer Treat Res*. 2019;177:63-80.
5. Cohen J, and Torres C. HIV-associated cellular senescence: A contributor to accelerated aging. *Ageing Res Rev*. 2017;36:117-24.
6. Montano M, Oursler KK, Xu K, Sun YV, and Marconi VC. Biological ageing with HIV infection: evaluating the geroscience hypothesis. *Lancet Healthy Longev*. 2022;3(3):e194-e205.
7. Guo J, Huang X, Dou L, Yan M, Shen T, Tang W, et al. Aging and aging-related diseases: from molecular mechanisms to interventions and treatments. *Signal Transduct Target Ther*. 2022;7(1):391.
8. Childs BG, Durik M, Baker DJ, and van Deursen JM. Cellular senescence in aging and age-related disease: from mechanisms to therapy. *Nat Med*. 2015;21(12):1424-35.
9. Nakanjako D, Nabatanzi R, Ssinabulya I, Bayigga L, Kiragga A, Banturaki G, et al. Chronic immune activation and accelerated immune aging among HIV-infected adults receiving suppressive antiretroviral therapy for at least 12 years in an African cohort. *Heliyon*. 2024;10(11):e31910.

- 784 10. Thangaraj A, Chivero ET, Tripathi A, Singh S, Niu F, Guo ML, et al. HIV TAT-mediated microglial
785 senescence: Role of SIRT3-dependent mitochondrial oxidative stress. *Redox Biol.*
786 2021;40:101843.
- 787 11. May T, Butueva M, Bantner S, Markusic D, Seppen J, MacLeod RA, et al. Synthetic gene
788 regulation circuits for control of cell expansion. *Tissue Eng Part A.* 2010;16(2):441-52.
- 789 12. Hwang HJ, Lee YR, Kang D, Lee HC, Seo HR, Ryu JK, et al. Endothelial cells under therapy-induced
790 senescence secrete CXCL11, which increases aggressiveness of breast cancer cells. *Cancer Lett.*
791 2020;490:100-10.
- 792 13. Abdelgawad IY, Agostinucci K, Ismail SG, Grant MKO, and Zordoky BN. EA.hy926 Cells and
793 HUVECs Share Similar Senescence Phenotypes but Respond Differently to the Senolytic Drug
794 ABT-263. *Cells.* 2022;11(13).
- 795 14. Brulois KF, Chang H, Lee AS, Ensser A, Wong LY, Toth Z, et al. Construction and manipulation of a
796 new Kaposi's sarcoma-associated herpesvirus bacterial artificial chromosome clone. *J Virol.*
797 2012;86(18):9708-20.
- 798 15. Greene W, and Gao SJ. Actin dynamics regulate multiple endosomal steps during Kaposi's
799 sarcoma-associated herpesvirus entry and trafficking in endothelial cells. *PLoS Pathog.*
800 2009;5(7):e1000512.
- 801 16. van der Meulen E, Anderton M, Blumenthal MJ, and Schafer G. Cellular receptors involved in
802 KSHV infection. *Viruses.* 2021;13(1).
- 803 17. Zou H, Stoppani E, Volonte D, and Galbiati F. Caveolin-1, cellular senescence and age-related
804 diseases. *Mech Ageing Dev.* 2011;132(11-12):533-42.
- 805 18. Park WY, Park JS, Cho KA, Kim DI, Ko YG, Seo JS, et al. Up-regulation of caveolin attenuates
806 epidermal growth factor signaling in senescent cells. *J Biol Chem.* 2000;275(27):20847-52.

- 807 19. Volonte D, and Galbiati F. Caveolin-1, a master regulator of cellular senescence. *Cancer*
808 *Metastasis Rev.* 2020;39(2):397-414.
- 809 20. Geng L, Liu Z, Zhang W, Li W, Wu Z, Wang W, et al. Chemical screen identifies a geroprotective
810 role of quercetin in premature aging. *Protein Cell.* 2019;10(6):417-35.
- 811 21. Akula SM, Pramod NP, Wang FZ, and Chandran B. Integrin alpha3beta1 (CD 49c/29) is a cellular
812 receptor for Kaposi's sarcoma-associated herpesvirus (KSHV/HHV-8) entry into the target cells.
813 *Cell.* 2002;108(3):407-19.
- 814 22. Veettil MV, Sadagopan S, Sharma-Walia N, Wang FZ, Raghu H, Varga L, et al. Kaposi's sarcoma-
815 associated herpesvirus forms a multimolecular complex of integrins (alphaVbeta5, alphaVbeta3,
816 and alpha3beta1) and CD98-xCT during infection of human dermal microvascular endothelial
817 cells, and CD98-xCT is essential for the postentry stage of infection. *J Virol.* 2008;82(24):12126-
818 44.
- 819 23. Hahn A, Birkmann A, Wies E, Dorer D, Mahr K, Sturzl M, et al. Kaposi's sarcoma-associated
820 herpesvirus gH/gL: glycoprotein export and interaction with cellular receptors. *J Virol.*
821 2009;83(1):396-407.
- 822 24. Boshoff C. Ephrin receptor: a door to KSHV infection. *Nat Med.* 2012;18(6):861-3.
- 823 25. Chen J, Zhang X, Schaller S, Jardetzky TS, and Longnecker R. Ephrin receptor A4 is a new Kaposi's
824 sarcoma-associated herpesvirus virus entry receptor. *mBio.* 2019;10(1).
- 825 26. Porta JC, Han B, Gulsevin A, Chung JM, Peskova Y, Connolly S, et al. Molecular architecture of the
826 human caveolin-1 complex. *Sci Adv.* 2022;8(19):7232.
- 827 27. Raghu H, Sharma-Walia N, Veettil MV, Sadagopan S, and Chandran B. Kaposi's sarcoma-
828 associated herpesvirus utilizes an actin polymerization-dependent macropinocytic pathway to
829 enter human dermal microvascular endothelial and human umbilical vein endothelial cells. *J*
830 *Virol.* 2009;83(10):4895-911.

- 831 28. Raghu H, Sharma-Walia N, Veettil MV, Sadagopan S, Caballero A, Sivakumar R, et al. Lipid rafts
832 of primary endothelial cells are essential for Kaposi's sarcoma-associated herpesvirus/human
833 herpesvirus 8-induced phosphatidylinositol 3-kinase and RhoA-GTPases critical for microtubule
834 dynamics and nuclear delivery of viral DNA but dispensable for binding and entry. *J Virol*.
835 2007;81(15):7941-59.
- 836 29. Kerur N, Veettil MV, Sharma-Walia N, Sadagopan S, Bottero V, Paul AG, et al. Characterization of
837 entry and infection of monocytic THP-1 cells by Kaposi's sarcoma associated herpesvirus (KSHV):
838 role of heparan sulfate, DC-SIGN, integrins and signaling. *Virology*. 2010;406(1):103-16.
- 839 30. Bizet AA, Liu K, Tran-Khanh N, Saksena A, Vorstenbosch J, Finnson KW, et al. The TGF-beta co-
840 receptor, CD109, promotes internalization and degradation of TGF-beta receptors. *Biochim*
841 *Biophys Acta*. 2011;1813(5):742-53.
- 842 31. Lin M, Sutherland DR, Horsfall W, Totty N, Yeo E, Nayar R, et al. Cell surface antigen CD109 is a
843 novel member of the alpha(2) macroglobulin/C3, C4, C5 family of thioester-containing proteins.
844 *Blood*. 2002;99(5):1683-91.
- 845 32. Yamakawa D, Jia W, Kidoya H, Hosojima S, Torigata M, Zhang L, et al. Visualization of
846 proliferative vascular endothelial cells in tumors in vivo by imaging their partner of Sld5-1
847 promoter activity. *Am J Pathol*. 2018;188(5):1300-14.
- 848 33. Finnson KW, Tam BY, Liu K, Marcoux A, Lepage P, Roy S, et al. Identification of CD109 as part of
849 the TGF-beta receptor system in human keratinocytes. *FASEB J*. 2006;20(9):1525-7.
- 850 34. Di Bartolo DL, Cannon M, Liu YF, Renne R, Chadburn A, Boshoff C, et al. KSHV LANA inhibits TGF-
851 beta signaling through epigenetic silencing of the TGF-beta type II receptor. *Blood*.
852 2008;111(9):4731-40.

- 853 35. Liu Y, Sun R, Lin X, Liang D, Deng Q, and Lan K. Kaposi's sarcoma-associated herpesvirus-encoded
854 microRNA miR-K12-11 attenuates transforming growth factor beta signaling through
855 suppression of SMAD5. *J Virol.* 2012;86(3):1372-81.
- 856 36. Lei X, Zhu Y, Jones T, Bai Z, Huang Y, and Gao SJ. A Kaposi's sarcoma-associated herpesvirus
857 microRNA and its variants target the transforming growth factor beta pathway to promote cell
858 survival. *J Virol.* 2012;86(21):11698-711.
- 859 37. Choi HS, Jain V, Krueger B, Marshall V, Kim CH, Shisler JL, et al. Kaposi's sarcoma-associated
860 herpesvirus (KSHV) induces the oncogenic miR-17-92 cluster and down-regulates TGF-beta
861 signaling. *PLoS Pathog.* 2015;11(11):e1005255.
- 862 38. Roberts AB, and Wakefield LM. The two faces of transforming growth factor beta in
863 carcinogenesis. *Proc Natl Acad Sci U S A.* 2003;100(15):8621-3.
- 864 39. Massague J, and Sheppard D. TGF-beta signaling in health and disease. *Cell.* 2023;186(19):4007-
865 37.
- 866 40. Song S, Tchkonina T, Jiang J, Kirkland JL, and Sun Y. Targeting senescent cells for a healthier aging:
867 challenges and opportunities. *Adv Sci (Weinh).* 2020;7(23):2002611.
- 868 41. Bartleson JM, Radenkovic D, Covarrubias AJ, Furman D, Winer DA, and Verdin E. SARS-CoV-2,
869 COVID-19 and the aging immune system. *Nat Aging.* 2021;1(9):769-82.
- 870 42. Prasanth MI, Brimson JM, and Tencomnao T. Virus-induced senescence: A therapeutic target to
871 mitigate severe progression of SARS-COV-2. *Expert Opin Ther Targets.* 2023;27(4-5):263-7.
- 872 43. Seoane R, Vidal S, Bouzaher YH, El Motiam A, and Rivas C. The interaction of viruses with the
873 cellular senescence response. *Biology (Basel).* 2020;9(12).
- 874 44. Koopal S, Furuhielm JH, Jarviluoma A, Jaamaa S, Pyakurel P, Pussinen C, et al. Viral oncogene-
875 induced DNA damage response is activated in Kaposi sarcoma tumorigenesis. *PLoS Pathog.*
876 2007;3(9):1348-60.

877 45. Lee MS, Yuan H, Jeon H, Zhu Y, Yoo S, Shi S, et al. Human mesenchymal stem cells of diverse
878 origins support persistent infection with Kaposi's sarcoma-associated herpesvirus and manifest
879 distinct angiogenic, invasive, and transforming phenotypes. *mBio*. 2016;7(1):e02109-15.

880 46. DiMaio TA, Vogt DT, and Lagunoff M. KSHV requires vCyclin to overcome replicative senescence
881 in primary human lymphatic endothelial cells. *PLoS Pathog*. 2020;16(6):e1008634.

882 47. Leidal AM, Cyr DP, Hill RJ, Lee PW, and McCormick C. Subversion of autophagy by Kaposi's
883 sarcoma-associated herpesvirus impairs oncogene-induced senescence. *Cell Host Microbe*.
884 2012;11(2):167-80.

885 48. Ganem D. KSHV and the pathogenesis of Kaposi sarcoma: listening to human biology and
886 medicine. *J Clin Invest*. 2010;120(4):939-49.

887 49. Bloom SI, Islam MT, Lesniewski LA, and Donato AJ. Mechanisms and consequences of
888 endothelial cell senescence. *Nat Rev Cardiol*. 2023;20(1):38-51.

889 50. Ye F, Zhou F, Bedolla RG, Jones T, Lei X, Kang T, et al. Reactive oxygen species hydrogen peroxide
890 mediates Kaposi's sarcoma-associated herpesvirus reactivation from latency. *PLoS Pathog*.
891 2011;7(5):e1002054.

892 51. Gao R, Li T, Tan B, Ramos da Silva S, Jung JU, Feng P, et al. FoxO1 suppresses Kaposi's sarcoma-
893 associated herpesvirus lytic replication and controls viral latency. *J Virol*. 2019;93(3).

894 52. Li T, and Gao SJ. KSHV hijacks FoxO1 to promote cell proliferation and cellular transformation by
895 antagonizing oxidative stress. *J Med Virol*. 2023;95(3):e28676.

896 53. Dalecki AG, Greer BD, Duverger A, Strange EL, Carlin E, Wagner F, et al. Host T cell
897 dedifferentiation effects drive HIV-1 latency stability. *J Virol*. 2022;96(5):e0197421.

898 54. Yang W, Jackson B, and Zhang H. Identification of glycoproteins associated with HIV latently
899 infected cells using quantitative glycoproteomics. *Proteomics*. 2016;16(13):1872-80.

900 55. Blaauw MJT, Cristina Dos Santos J, Vadaq N, Trypsteen W, van der Heijden W, Groenendijk A, et
901 al. Targeted plasma proteomics identifies MICA and IL1R1 proteins associated with HIV-1
902 reservoir size. *iScience*. 2023;26(4):106486.

903 56. Schmitt CA, Wang B, and Demaria M. Senescence and cancer - role and therapeutic
904 opportunities. *Nat Rev Clin Oncol*. 2022;19(10):619-36.

905 57. Wang B, Kohli J, and Demaria M. Senescent cells in cancer therapy: friends or foes? *Trends*
906 *Cancer*. 2020;6(10):838-57.

907 58. Kang SK, Kang YH, Yoo SM, Park C, Kim HS, and Lee MS. HMGB1 knockout decreases Kaposi's
908 sarcoma-associated herpesvirus virion production in iSLK BAC16 cells by attenuating viral gene
909 expression. *J Virol*. 2021;95(16):e0079921.

910 59. Yoo SM, Ahn AK, Seo T, Hong HB, Chung MA, Jung SD, et al. Centrifugal enhancement of Kaposi's
911 sarcoma-associated virus infection of human endothelial cells in vitro. *J Virol Methods*.
912 2008;154(1-2):160-6.

913 60. Bottero V, Chakraborty S, and Chandran B. Reactive oxygen species are induced by Kaposi's
914 sarcoma-associated herpesvirus early during primary infection of endothelial cells to promote
915 virus entry. *J Virol*. 2013;87(3):1733-49.

916 61. Lee MJ, Park J, Choi S, Yoo SM, Park C, Kim HS, et al. HMGB1, a potential regulator of tumor
917 microenvironment in KSHV-infected endothelial cells. *Front Microbiol*. 2023;14:1202993.

918 62. Lee MS, Jones T, Song DY, Jang JH, Jung JU, and Gao SJ. Exploitation of the complement system
919 by oncogenic Kaposi's sarcoma-associated herpesvirus for cell survival and persistent infection.
920 *PLoS Pathog*. 2014;10(9):e1004412.

921 63. Kang SK, Lee MJ, Ryu HH, Lee J, and Lee MS. Dimethyl sulfoxide enhances Kaposi's sarcoma-
922 associated herpesvirus production during lytic replication. *Front Microbiol*. 2021;12:778525.

- 923 64. Lee MJ, Lee J, Kang SK, Wirth D, Yoo SM, Park C, et al. CXCL1 confers a survival advantage in
924 Kaposi's sarcoma-associated herpesvirus-infected human endothelial cells through STAT3
925 phosphorylation. *J Med Virol.* 2023;95(1).
- 926 65. Lee MS, Kim JH, Lee JS, Yun SJ, Kim WJ, Ahn H, et al. Prognostic significance of CREB-binding
927 protein and CD81 expression in primary high grade non-muscle invasive bladder cancer:
928 identification of novel biomarkers for bladder cancer using antibody microarray. *PLoS One.*
929 2015;10(4):e0125405.
- 930

Table 1. LC-MS/MS expression of KSHV receptor candidate in control and senescent HuARLT cells

Uniport ID	Abbreviation	cell lysate			cell pellet		
		Control (%mol)	Senescence (%mol)	fold change	Control (%mol)	Senescence (%mol)	fold change
P09601	HO-1	0.0069	0.035	5.07	0.0022	0.0173	7.86
Q03135	Cav-1	0.0093	0.0261	2.81	0.0036	0.0264	7.33
P17301	ITG- α 2	0.0003	0.0089	29.67	0.0003	0.0009	3.00
P07237	P4HB	0.0984	0.2678	2.72	0.0528	0.0913	1.73
Q9Y624	F11R	0.0069	0.016	2.32	0.0021	0.0043	2.05
P50552	VASP	0.0203	0.0445	2.19	0.0031	0.0045	1.45
Q6YHK3	CD109	0.0009	0.0119	13.22	0.0048	0.0107	2.23

Table 2. Assessment of CD109 RNA expression changes with aging in *Macaca fascicularis* and *Homo sapiens*. The percent change (% change) is derived from conversion of Avg_logFC values.

<i>Macaca fascicularis</i> (Crab-eating macaque)					
Tissue	Cell type	Avg_logFC	% change	Method	DOI
Lung	Venous endothelial cell	0.355605	28.5%	sc-RNA-Seq	10.1038/s41422-020-00412-6
Heart	Arterial endothelial cell	0.3918	30.6%	sc-RNA-Seq	10.1038/s41422-020-00412-6
Retina	Endothelial cell	-1.36321	-48.4%	sc-RNA-Seq	10.1007/s13238-020-00791-x
Liver	Endothelial cell	0.673593	62%	sc-RNA-Seq	10.1093/procel/pwad039
Adrenal gland	Endothelial cell	0.355082	28.5%	sc-RNA-Seq	10.1038/s43587-024-00588-1
Lung	Venous endothelial cell	0.355605	28.5%	sc-RNA-Seq	10.1038/s41422-020-00412-6
<i>Homo sapiens</i>					
Tissue	Cell type	Avg_logFC	% change	Method	DOI
Skin	Fibroblast	0.330582	25.75%	sc-RNA-Seq	10.1016/j.devcel.2020.11.002
Cell (In vitro)	Umbilical vein endothelial cells	1.25311	138.35%	RNA-Seq	10.1038/s43587-021-00151-2

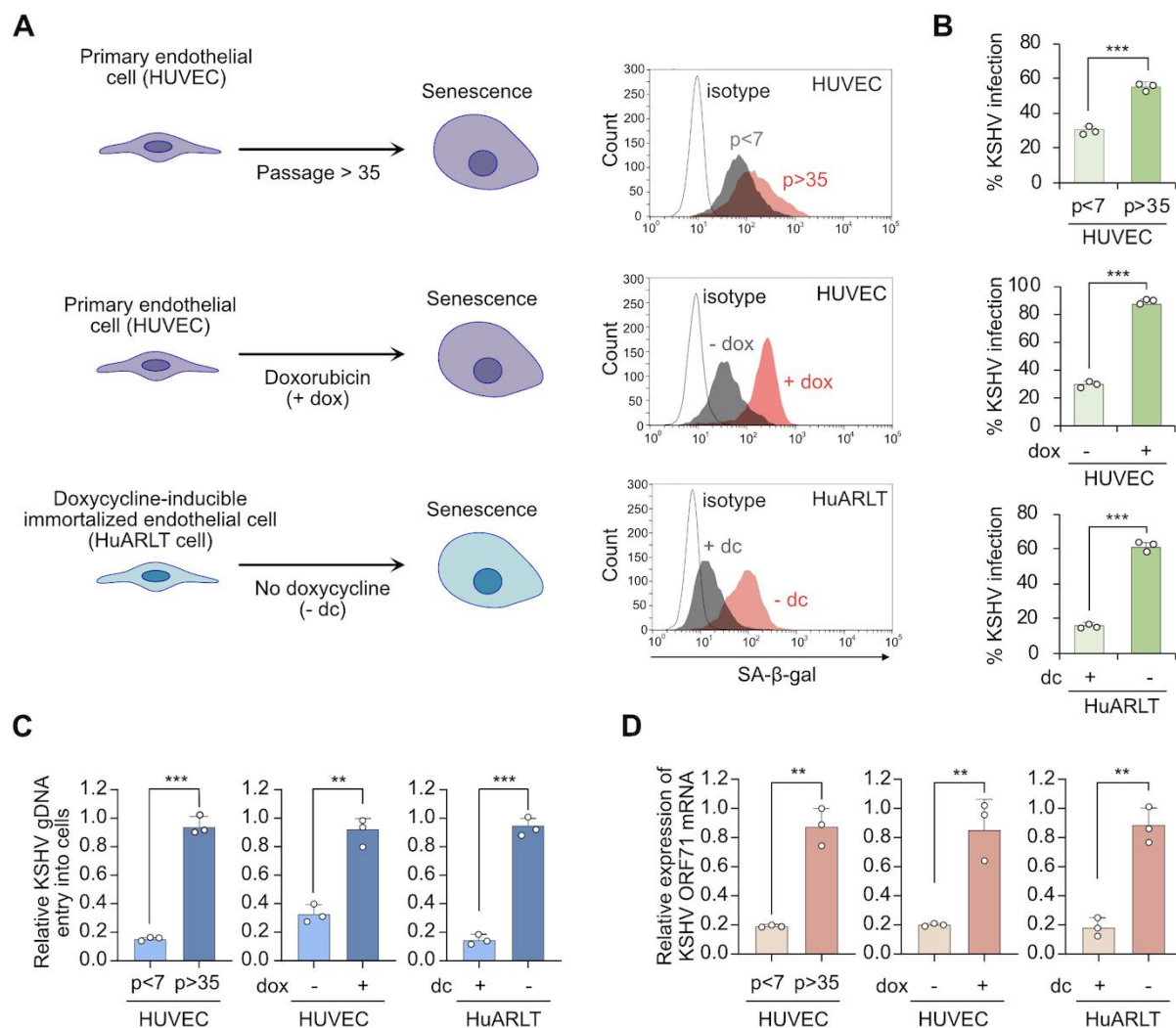


Figure 1. Increased KSHV infection in senescent human endothelial cells. (A)

Senescence was induced in primary human endothelial cells (HUVECs) by repeated subculture over 35 passages or treatment with doxorubicin. In doxycycline-inducible immortalized human endothelial cells (HuARLT cells), senescence was induced by culturing without doxycycline. SA-β-gal staining was used for validation of senescence through microscopy or flow cytometry. p, cell culture passages. KSHV infectivity was measured by GFP expression in cells infected with recombinant KSHV BAC16. (B)

947 Analysis of KSHV-infected cells in non-senescent and senescent human endothelial cells
948 by flow cytometry 24 hours postinfection. Data are representative of 3 independent
949 experiments. Data are shown as mean \pm SD, N = 3; *** p < 0.001 using unpaired 2-tailed
950 Student's t test. **(C)** Quantification of the KSHV genome in KSHV-infected non-senescent
951 and senescent human endothelial cells by quantitative PCR 24 hours postinfection. Data
952 are representative of 3 independent experiments. Data are shown as mean \pm SD, N = 3;
953 ** p < 0.01, *** p < 0.001 using unpaired 2-tailed Student's t test. **(D)** Assessment of the
954 relative expression of KSHV *ORF71* mRNA in KSHV-infected non-senescent and
955 senescent human endothelial cells using quantitative reverse transcription PCR 24 hours
956 postinfection. Data are representative of 3 independent experiments. Data are shown as
957 mean \pm SD, N = 3; ** p < 0.01 using unpaired 2-tailed Student's t test.

958

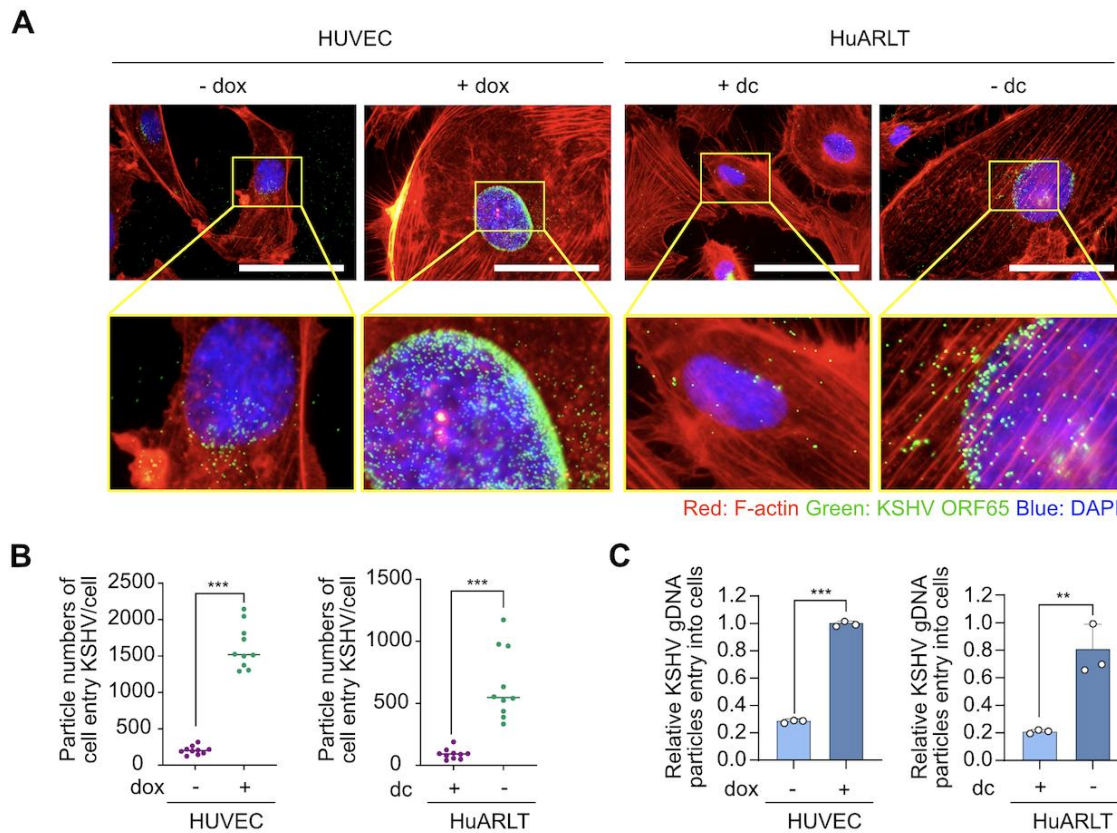


Figure 2. Enhanced entry of KSHV in senescent human endothelial cells. (A)

Immunofluorescence assay of the entry of KSHV into non-senescent and senescent cells. KSHV was visualized 4 hours postinfection using KSHV ORF65 antibody. Phalloidin (F-actin) and DAPI were used to visualize the shapes of the cells and nuclei, respectively. Scale bar, 50 μm. (B) Analysis of the number of internalized KSHV particles per cell in the images in (A) and Supplemental Figure 5. Data are representative of 10 independent experiments. Data are shown as mean ± SD, N = 10; *** $p < 0.001$ using unpaired 2-tailed Student's t test. (C) Quantification of the internalized KSHV genome in the KSHV-infected non-senescent and senescent human endothelial cells by quantitative PCR. Genomic DNA was extracted from KSHV-infected cells 4 hours postinfection. The KSHV genome

970 was quantified in the extracted DNA by quantitative PCR using primers for KSHV ORF26.

971 Data are representative of 3 independent experiments. Data are shown as mean \pm SD, N

972 = 3; ** $p < 0.01$, *** $p < 0.001$ using unpaired 2-tailed Student's t test.

973

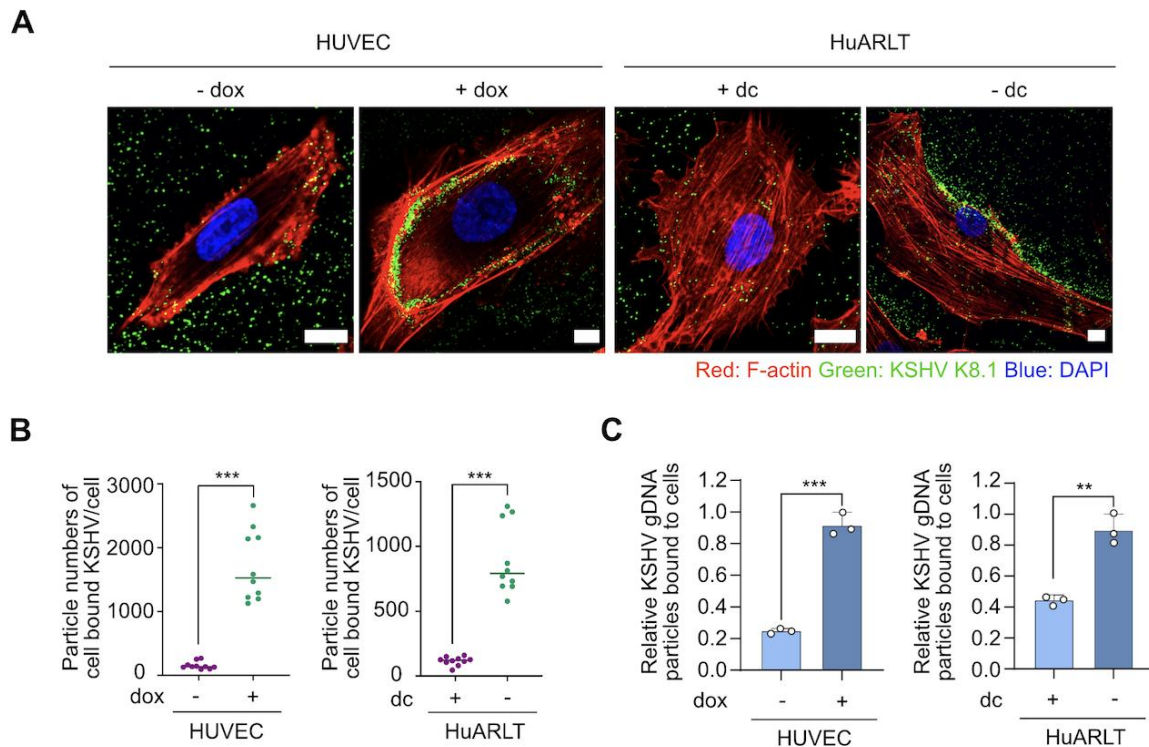


Figure 3. Enhanced binding of KSHV in senescent human endothelial cells. (A)

Confocal microscopy images of KSHV binding to the cell surface. After infection, cells were immediately fixed and stained without permeabilization. Scale bar, 10 μ m. **(B)**

Analysis of the number of KSHV particles binding to the cell surface per cell in the images in (A) and Supplemental Figure 6. Data are representative of 10 independent experiments.

Data are shown as mean \pm SD, N = 10; *** p < 0.001 using unpaired 2-tailed Student's t

test. **(C)** Quantification of the cell surface-bound KSHV genome in KSHV-infected cells

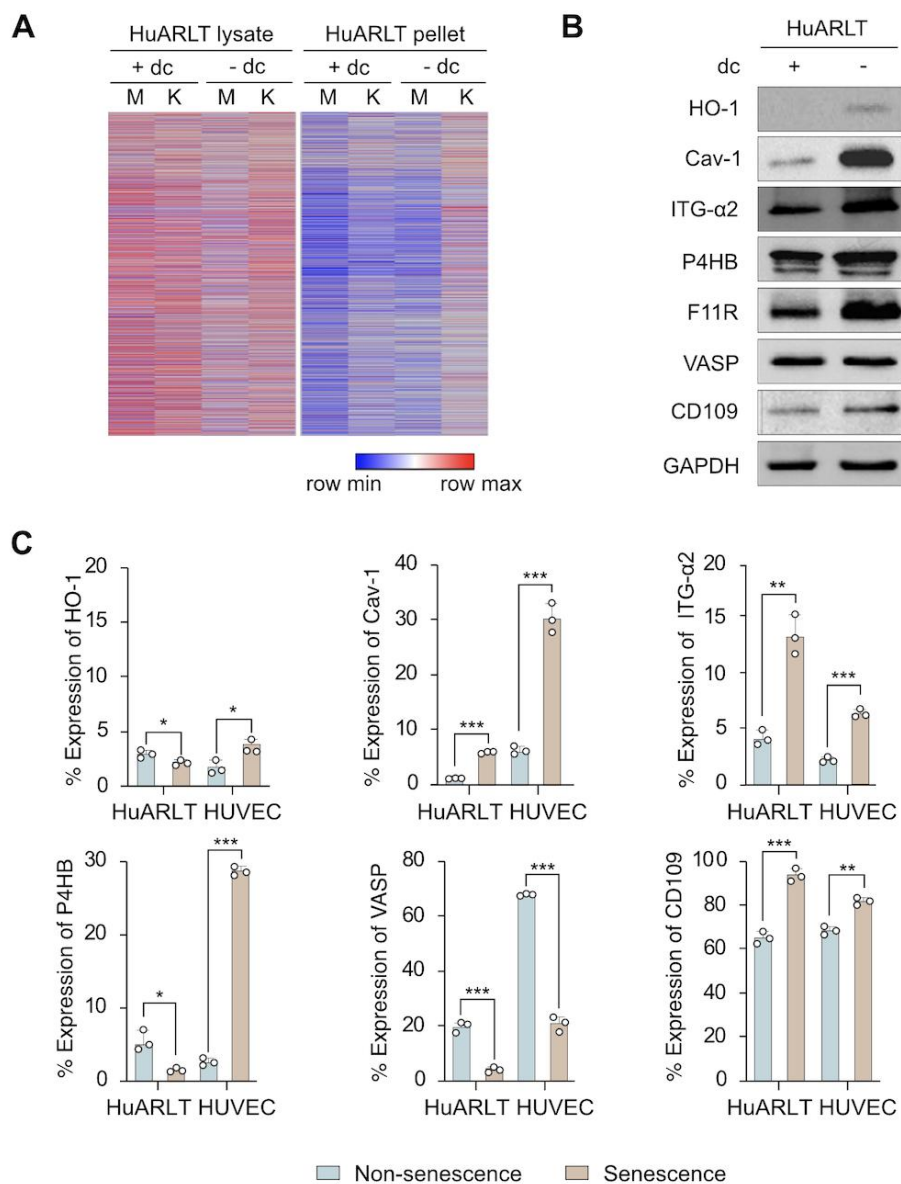
by quantitative PCR. After 1 hour of KSHV infection, the cells were immediately scraped

and genomic DNA was extracted. The KSHV genome was quantified in the extracted

DNA by quantitative PCR using primers for KSHV ORF26. Data are representative of 3

985 independent experiments. Data are shown as mean \pm SD, N = 3; ** p < 0.01, *** p < 0.001
986 using unpaired 2-tailed Student's t test.

987



988

989 **Figure 4. Identification of candidate proteins associated with increased KSHV**

990 **infectivity in senescent endothelial cells. (A)** Heatmap of the differential expression of

991 proteins from non-senescent (+dc, culture with doxycycline) and senescent (-dc, culture

992 without doxycycline) HuARLT cells with KSHV (K) or without KSHV (M). The cell lysate

993 and cell pellet from each conditioned cell were analyzed by LC-MS/MS. **(B)** Western blot

994 analysis of the selected candidate proteins. Cav-1, caveolin-1; ITG, integrin; dc,
995 doxycycline. GAPDH was used as a housekeeping protein for normalization. (C) Flow
996 cytometric analysis of candidate proteins in non-senescent (+dc HuARLT and -dox
997 HUVEC) and senescent (-dc HuARLT and +dox HUVEC) cells. Data are representative
998 of 3 independent experiments. Data are shown as mean \pm SD, N = 3; * p < 0.05, ** p <
999 0.01, *** p < 0.001, ns: not significant using unpaired 2-tailed Student's t test.

1000

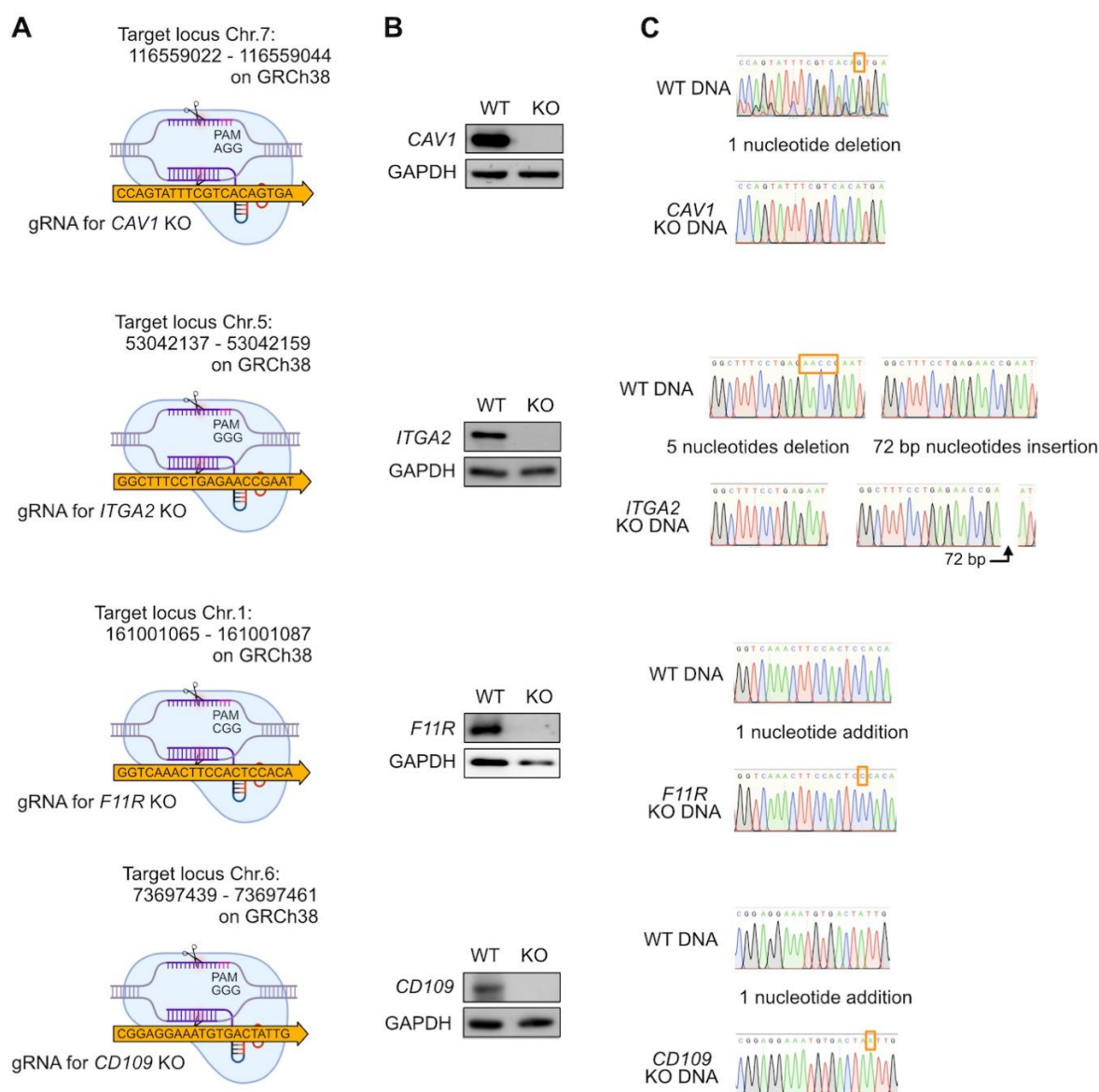


Figure 5. Establishment and characterization of knockout clones for the candidate proteins in HuARLT cells. (A) Schematic diagram of the guide RNA (gRNA) sequence for caveolin-1 (*CAV1*), integrin $\alpha 2$ (*ITGA2*), *F11R*, and *CD109*. The gRNA-recognizing site is indicated as the CRISPR target sequence. (B) Western blot analysis of each knockout protein. WT, wild-type HuARLT cell; KO, knockout HuARLT cell. (C) Target sequence analysis in WT and KO HuARLT cells. The PCR products containing the gRNA

1008 targeting region from the genomic DNA of WT and KO cells were cloned into a T-vector.
1009 The sequences of 10 colonies were analyzed by Sanger sequencing. The mutated region
1010 is indicated by a box.

1011

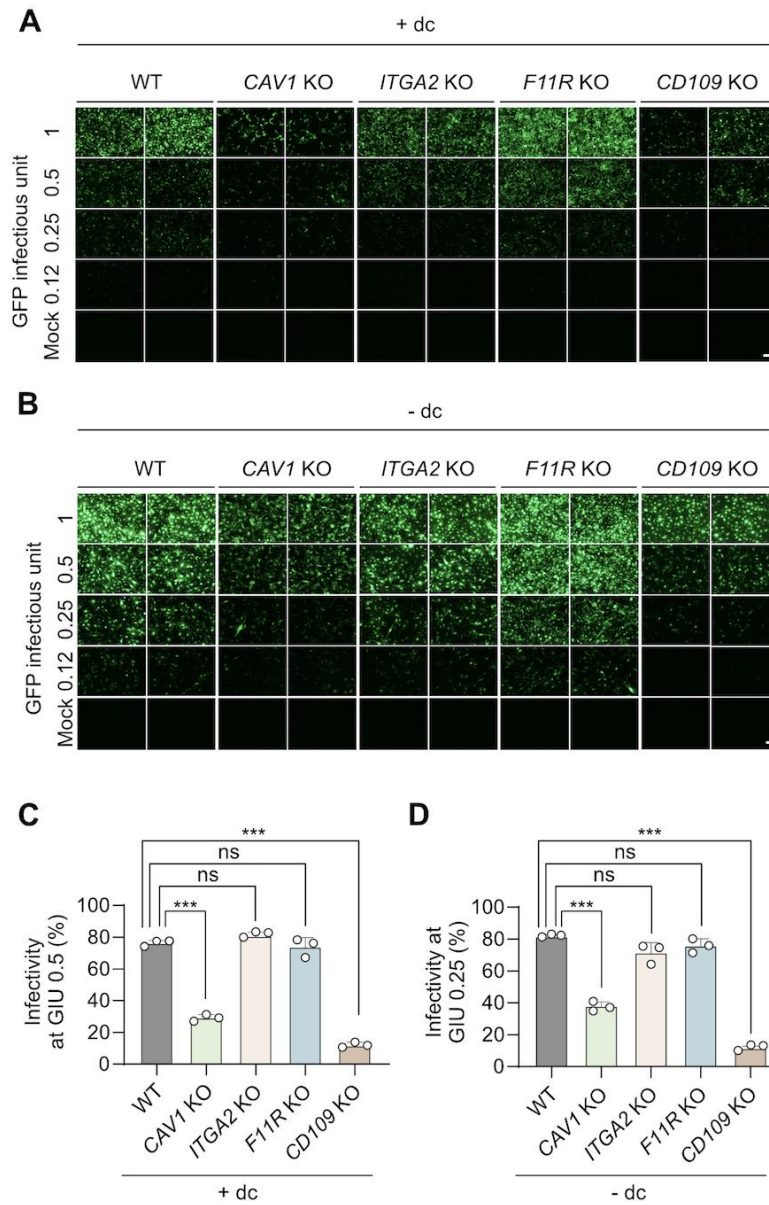


Figure 6. Analysis of KSHV infectivity in knockout clones of *CAV1*, *ITGA2*, *F11R*, and *CD109*. An equivalent quantity of KSHV was used to infect the same number of wild-type (WT) and knockout (KO) HuARLT cells, with or without induction of senescence. KSHV was prepared as GFP infectious units of 1 to infect approximately 90% of non-senescent WT cells, followed by the infection of a 2-fold serially diluted virus into each

1018 group of conditioned cells. KSHV infectivity was measured using GFP expression. (**A** and
1019 **B**) Fluorescence microscopic visualization of KSHV-infected cells for each KO clone in
1020 non-senescent (+dc, **A**) and senescent (-dc, **B**) HuARLT cells. *CAV1*, caveolin-1; *ITGA2*,
1021 integrin- α 2. Scale bar, 100 μ m. (**C** and **D**) Flow cytometric analysis of KSHV-infected cells
1022 for each KO clone in non-senescent (+dc, **C**) and senescent (-dc, **D**) HuARLT cells. At
1023 the indicated GFP infectious units (GIU), the percentage of KSHV-infected cells was
1024 compared among each group. Data are representative of 3 independent experiments.
1025 Data are shown as mean \pm SD, N = 3; *** p < 0.001, ns: not significant using Dunnett's
1026 test for multiple comparisons.

1027

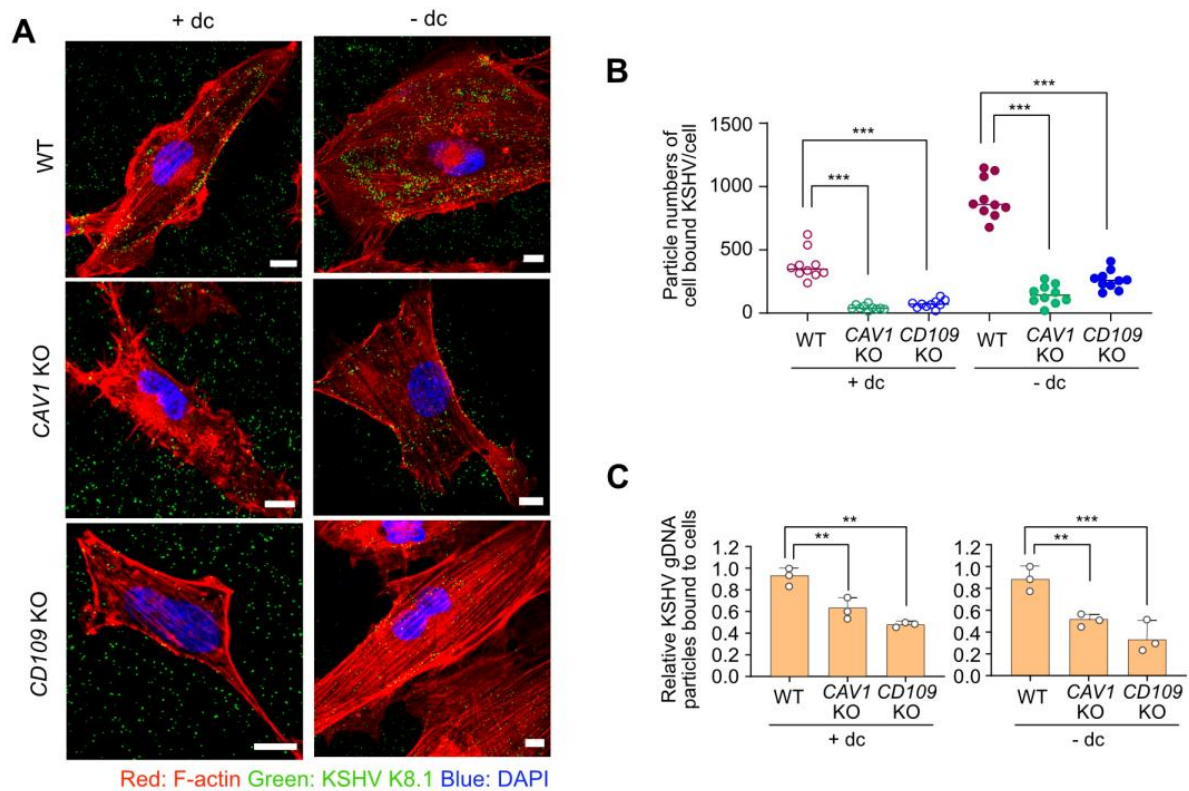


Figure 7. KSHV binding to the cell surface of *CAV1* KO and *CD109* KO HuARLT cells.

(A) Representative confocal images of KSHV virus particles in *CAV1* KO and *CD109* KO HuARLT cells. Scale bar, 10 μ m. (B) Analysis of the number of KSHV particles that bind to the cell surface per cell in the images in (A) and Supplemental Figure 13. Data are representative of 10 independent experiments. Data are shown as mean \pm SD, N = 10; *** p < 0.001 using Dunnett's test for multiple comparisons. (C) Quantification of the cell surface-bound KSHV genome in the KSHV-infected cells by quantitative PCR. After 1 hour of KSHV infection, the cells were immediately scraped, and genomic DNA extracted after washing. The KSHV genome was quantified in the extracted DNA by quantitative PCR using primers for KSHV ORF26. Data are representative of 3 independent

1039 experiments. Data are shown as mean \pm SD, N = 3; ** p < 0.01, *** p < 0.001 using
1040 Dunnett's test for multiple comparisons.

1041

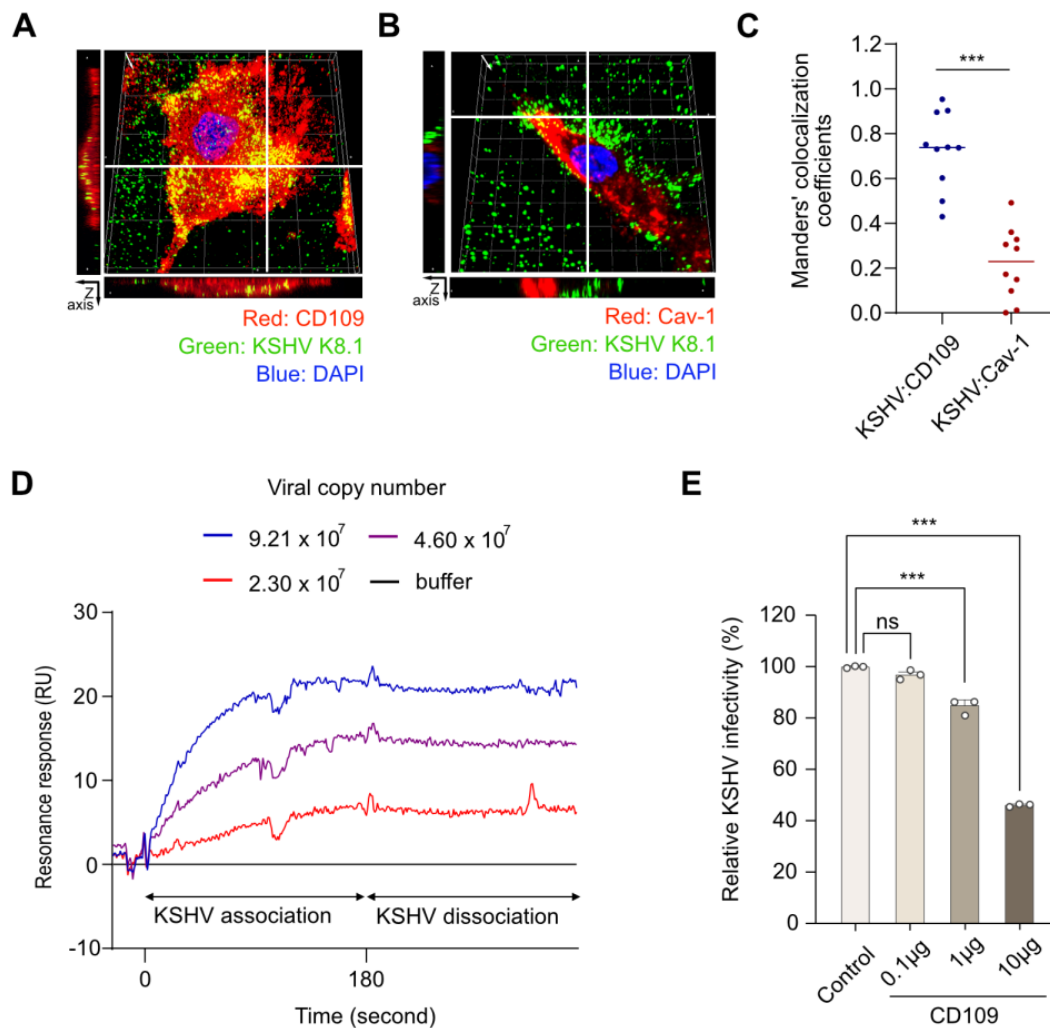


Figure 8. Analysis of KSHV interaction with caveolin-1 and CD109. (A and B) Three-dimensional confocal microscopy images of the colocalization of KSHV with CD109 (A) or caveolin-1 (Cav-1) (B). Senescent HuARLT cells infected with KSHV for 1 hour were stained with KSHV K8.1 antibody and target proteins, and Z-axis scanning was performed at 4 µm intervals, generating more than 10 scans. The bar-shaped images at the edges represent cross-sections, guided by white solid lines in the stacked image. (C) Quantitative analysis of the colocalization of KSHV with CD109 or caveolin-1 by Manders' colocalization coefficient in KSHV-infected senescent HuARLT cells. N = 10; ****p* < 0.001

1051 (D) SPR analysis of KSHV binding to immobilized recombinant CD109. Data are
1052 representative of 3 independent experiments. (E) Neutralization of KSHV infectivity using
1053 a recombinant CD109 protein. Data are representative of 3 independent experiments.
1054 Data are presented as mean \pm SD, N = 3; *** $p < 0.001$ ns: not significant using Dunnett's
1055 test for multiple comparisons.

1056

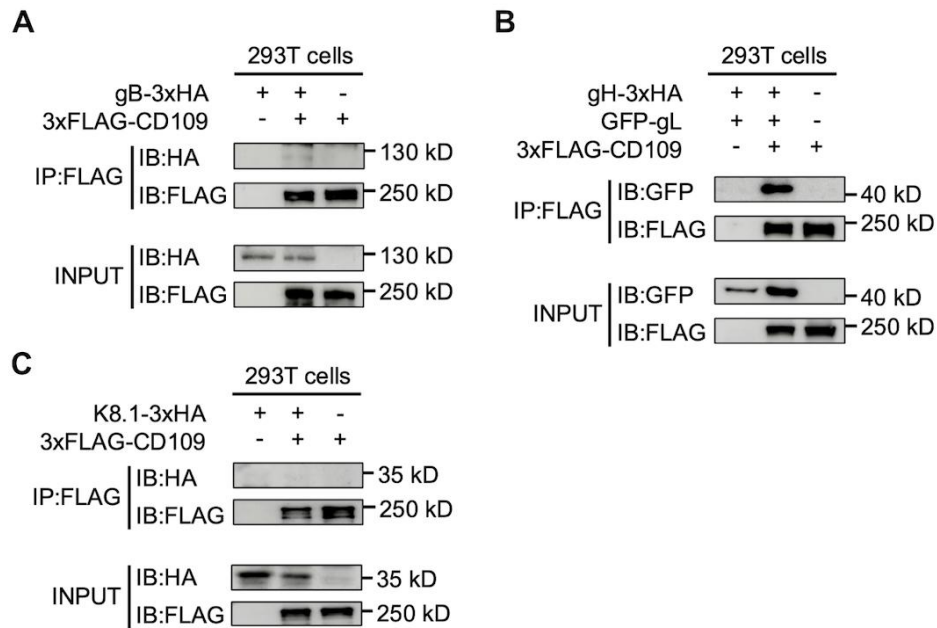


Figure 9. KSHV gH/gL interacts with CD109. Co-immunoprecipitation analysis of CD109 with KSHV glycoproteins gB (A), gH/gL (B), and K8.1 (C). HEK-293T cells were co-transfected with the indicated plasmids for 24 hours, after which cell lysates were subjected to immunoprecipitation (IP) using anti-FLAG magnetic agarose beads. The resulting complexes were then analyzed by immunoblotting (IB) using the indicated antibodies. Data are representative of 3 independent experiments